JACS
JOURNAL OF THE AMERICAN CHEMICAL SOCIETY

ARTICLE

pubs.acs.org/JACS

Poly(perfluoroalkylation) of Metallic Nitride Fullerenes Reveals Addition-Pattern Guidelines: Synthesis and Characterization of a Family of $Sc_3N@C_{80}(CF_3)_n$ (n = 2−16) and Their Radical Anions

Natalia B. Shustova,[‡] Dmitry V. Peryshkov,[‡] Igor V. Kuvychko,[‡] Yu-Sheng Chen,[§] Mary A. Mackey,[¶] Curtis E. Coumbe,[¶] David T. Heaps,[¶] Bridget S. Confait,[¶] Thomas Heine,[⊥] J. Paige Phillips,*[,¶] Steven Stevenson,*[,¶] Lothar Dunsch,*[,†] Alexey A. Popov,*[,†] Steven H. Strauss,*[,‡] and Olga V. Boltalina*[,‡]

[‡]Department of Chemistry, Colorado State University, Fort Collins, Colorado 80523, United States

[§]ChemMatCARS Beamline, University of Chicago Advanced Photon Source, Argonne, Illinois 60439, United States

[¶]Department of Chemistry and Biochemistry, University of Southern Mississippi, Hattiesburg, Mississippi 39406, United States

[⊥]School of Engineering and Science, Jacobs University, D-28759 Bremen, Germany

[†]Department of Electrochemistry and Conducting Polymers, Leibniz Institute for Solid State and Materials Research, D-01069 Dresden, Germany

Supporting Information

ABSTRACT: A family of highly stable (poly)perfluoroalkylated metallic nitride cluster fullerenes was prepared in high-temperature reactions and characterized by spectroscopic (MS, ^{19}F NMR, UV−vis/NIR, ESR), structural and electrochemical methods. For two new compounds, $Sc_3N@C_{80}(CF_3)_{10}$ and $Sc_3N@C_{80}(CF_3)_{12}$, single crystal X-ray structures are determined. Addition pattern guidelines for endohedral fullerene derivatives with bulky functional groups are formulated as a result of experimental (^{19}F NMR spectroscopy and single crystal X-ray diffraction) studies and exhaustive quantum chemical calculations of the structures of $Sc_3N@C_{80}(CF_3)_n$ (n = 2-16). Electrochemical studies revealed that $Sc_3N@C_{80}(CF_3)_n$ derivatives are easier to reduce than $Sc_3N@C_{80}$, the shift of $E_{1/2}$ potentials ranging from +0.11 V (n = 2) to +0.42 V (n = 10). Stable radical anions of $Sc_3N@C_{80}(CF_3)_n$ were generated in solution and characterized by ESR spectroscopy, revealing their ^{45}Sc hyperfine structure. Facile further functionalizations via cycloadditions or radical additions were achieved for trifluoromethylated $Sc_3N@C_{80}$ making them attractive versatile platforms for the design of molecular and supramolecular materials of fundamental and practical importance.

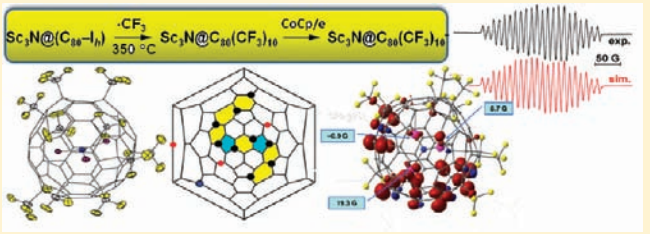

1. INTRODUCTION

More than a decade ago, a new class of endohedral metallofullerenes (or endometallofullerenes, EMFs) was discovered, metallic nitride cluster fullerenes (MNFs).[1] Due to later advances in synthetic routes,[2−6] large-scale synthesis, and isolation techniques,[2−6] these compounds have been actively studied by scientists from a wide range of research disciplines (for recent reviews see refs 7−9). Besides an obvious fundamental interest, MNFs show promise in various areas of practical importance such as biomedical research[10,11] and energy conversion.[12−14] In the latter, the development of organic photovoltaic (OPV) devices based on the use of fullerenes as electron acceptor materials has recently led to the fabrication and testing of the OPV devices with an MNF acceptor blended with the donor polymer P3HT. Due to a better separation between LUMO level of the acceptor and HOMO level of the donor, these devices showed high power conversion efficiency, rivaling that of PCBM/P3HT-based devices.[15] Among several critical issues that have to be solved before MNF-based OPV devices become commercially viable are the improvements in processability (which involves improved solubility of MNFs and higher stability of the films and solutions), optimization of the morphology of the blends, and optimization of the electronic properties of the donor and fullerene acceptor, i.e., bandgap engineering (to ensure the most efficient exciton separation and light harvesting). In the biomedical field,[10,11] precisely controlled derivatization of MNFs is one of the keys to successful advancements toward practical applications that may result in new concepts such as "bio-shuttle" systems. Overall, innovative methods of functionalization of MNFs need to be developed to satisfy the needs of emerging technological applications. In contrast to the well-developed mono-cycloadditions to MNFs and to less

Received: October 30, 2010
Published: February 4, 2011

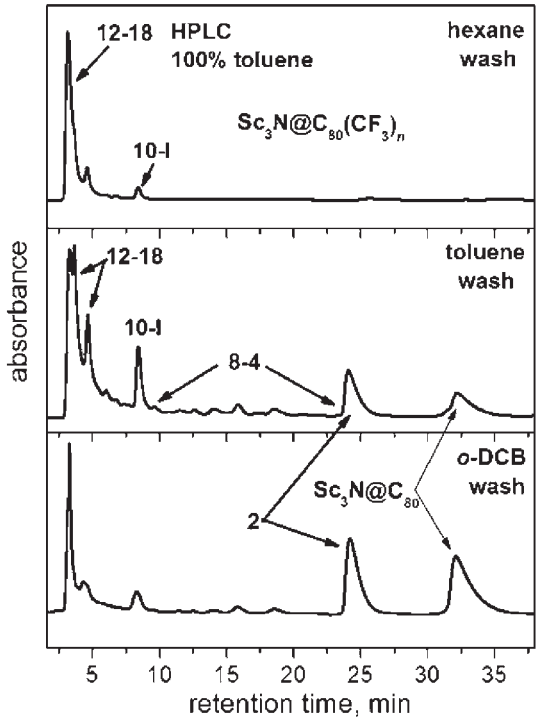

Figure 1. HPLC traces of the $Sc_3N@(C_{80}\text{-}I_h)(CF_3)_n$ products obtained as a result of a three-step extraction involving washing with hexane (top), toluene (middle), and *o*-dichlorobenzene (bottom).

well-developed bis-cycloadditions,[8] the chemistry of multiple additions to MNFs still remains in its infancy[16−18] (see Supporting Information [SI]).

This paper describes a comprehensive study of various polyadditions to MNFs that covers several key areas: (i) reactions of MNFs with various radicals generated either thermally or photochemically; (ii) isolation of many pure isomers of MNF derivatives and their complete spectroscopic and structural characterization (including single-crystal X-ray crystallography); (iii) studies of physical and chemical properties of $MNF(CF_3)_n$ derivatives; (iv) studies of electronic properties of well-characterized $MNF(CF_3)_n$ that included UV−vis/NIR spectroscopy, electrochemical properties, and ESR studies of the corresponding radical anions produced by chemical or electrochemical reduction; and (v) a comprehensive theoretical study including structures, stability, frontier orbital analysis, simulation of spectroscopic data, and comparison with experimental spectroscopic results.

2. RESULTS AND DISCUSSION

2.1. Synthesis and Isolation of $Sc_3N@C_{80}(CF_3)_n$. A series of preliminary trifluoromethylation reactions was carried out using different reagents, reaction parameters (such as temperature and time), reactor types, and samples of $Sc_3N@C_{80}$ of varying purity in order to determine optimal conditions (see description in SI-I).

One of the trifluoromethylating agents that afforded good yields and conversion in reactions with pure samples of $Sc_3N@(C_{80}\text{-}I_h)$ was CF_3COOAg (AgTFA). In a previous study, the trifluoromethylation of $Y@C_{82}$-containing extract with 25 equiv of AgTFA resulted in the selective formation of two isomers of $Y@C_{82}(CF_3)_5$.[19] In this work, reactions of $Sc_3N@(C_{80}\text{-}I_h)$ with 50 equiv of AgTFA were carried out in a sealed reactor at 350 °C for 2.5 h as described earlier.[20] Increase of the reaction temperature up to 450 °C led to a drastic decrease in the yield of $Sc_3N@(C_{80}\text{-}I_h)(CF_3)_n$ compounds, possibly because of the thermal degradation of AgTFA prior to the reaction and/or partial thermal degradation of $Sc_3N@(C_{80}\text{-}I_h)(CF_3)_n$. The $Sc_3N@(C_{80}\text{-}I_h)(CF_3)_n$ products were separated from the inorganic residues using the three-solvent extraction procedure (see Figure 1 and [SI]). Partial separation of $Sc_3N@(C_{80}\text{-}I_h)(CF_3)_n$ products was achieved at each extraction stage. The first hexane wash extracted highly trifluoromethylated products with n = 10−18 (see Figure 1, top); the second toluene wash extracted most of the trifluoromethylated products with a wide range of compositions (n = 2−18, the most abundant compounds contained 12 and 14 CF_3 groups, see Figure 1, middle); the final *o*-dichlorobenzene wash extracted **Sc-2-1** isomer and unreacted $Sc_3N@(C_{80}\text{-}I_h)$ (Figure 1, bottom). [The following abbreviations were adopted for TMF isomers, addition patterns for which have been unambiguously determined by X-ray crystallography or ^{19}F NMR spectroscopy. In the case of hollow fullerenes, the abbreviation, e.g., **60-8-2**, is deconvoluted as follows: the first number (60) is the carbon cage, the second number (8) is the number of R_f groups, the third number (2) is the isomer number. By default, $R_f = CF_3$; in other cases R_f is added at the end of the abbreviation. Similar notations are used for MNFs; in **Sc-2-1**, e.g., (Sc) denotes the Sc_3N cluster type; (2) is the number of R_f groups (by default $R_f = CF_3$), and (1) is the isomer number.] In contrast to underivatized MNFs, which have notoriously low solubilities in most organic solvents, the $Sc_3N@(C_{80}\text{-}I_h)(CF_3)_n$ compounds with a large number of CF_3 groups (n = 10−18) are highly soluble in aliphatic solvents (heptane or hexane), whereas compounds with $2 < n < 12$ groups also have good solubility in aromatic solvents (benzene, toluene or *o*-dichlorobenzene). For example, the results of the dynamic light scattering (DLS) study of toluene solutions of C_{60}, $Sc_3N@C_{80}$ and $Sc_3N@C_{80}(CF_3)_{12-14}$ samples are provided in Table 1. Unfunctionalized C_{60} and $Sc_3N@C_{80}$ form large aggregates with broad particle size distributions; however, derivatization with multiple CF_3 groups, as in $Sc_3N@C_{80}(CF_3)_{12-14}$, deters aggregation, and the samples characterized by very narrow size distributions are produced. This increased solubility may contribute to the enhanced reactivity and selectivity observed in subsequent functionalization reactions of $Sc_3N@C_{80}(CF_3)_n$.

Table 1. Dynamic Light Scattering (DLS) Results of Toluene Solutions of Selected Fullerenes and Fullerene Derivatives

sample	concentration (mM)	average particle size (nm)
C_{60}	0.2	460(113), 475(103), 438(40)
$Sc_3N@C_{80}$	0.2	595(91), 889(86), 712(156)
$Sc_3N@C_{80}(CF_3)_{12-14}$	0.2	1.9(0.2), 1.8(0.2), 1.8(0.2)

In the AgTFA reaction, the maximum number of CF_3 groups (n_{max}) that attached to the $Sc_3N@(C_{80}\text{-}I_h)$ cage was 18, which corresponds to the conversion of 22% of the sp^2 cage carbon atoms into sp^3 hybridized carbon atoms. For comparison, in the analogous AgTFA reactions with C_{60}, the observed n_{max} value was 22, which corresponds to the transformation of 37% of sp^2 carbon cage atoms into sp^3 carbon atoms.[21,22] This apparent lower addition degree to MNF than to a hollow fullerene with smaller cage size will be discussed later in the text.

dx.doi.org/10.1021/ja109462j |*J. Am. Chem. Soc.* 2011, 133, 2672–2690

To achieve a higher degree of trifluoromethylation, a crude mixture of $Sc_3N@(C_{80}\text{-}I_h)(CF_3)_n$ ($n = 2-18$) was subjected to the second round of the AgTFA treatment (~140 equiv of AgTFA were used, other reaction conditions were kept the same). Surprisingly, only a small shift of the composition toward higher n values was observed according to the NI atmospheric pressure photoionization mass spectrometry (APPI MS); n_{max} was found to be equal to 20 and species with $n = 16$ became the most abundant in the new product. The HPLC trace showed the absence of the compounds with retention times longer than 4 min, which was indicative that the molecules with $n < 12$ were trifluoromethylated further and converted into the products with the higher n values (Figure SI-1 [SI]). Therefore, the maximum number of sp^3 carbons bearing CF_3 radicals still did not exceed 25%. In the case of cycloaddition of malonate free radicals to $Sc_3N@(C_{80}\text{-}I_h)$, Dorn and co-workers observed octaadducts, and for $Lu_3N@(C_{80}\text{-}I_h)$, deca-adducts were detected. This corresponds to the formation of 20% and 25% of sp^3 hybridized carbons per cage, respectively.[23] Interestingly, trifluoromethylation of monometallofullerene $Y@C_{82}$ (as DMF extract) with the large excess of AgTFA resulted in the selective formation of $Y@C_{82}(CF_3)_5$ isomers, whereas molecules with higher n values were not observed at all.[19]

A good solubility of $Sc_3N@(C_{80}\text{-}I_h)(CF_3)_n$ in various organic solvents and high stability of these solutions under air allowed us to use HPLC as the primary method for isolation and purification of isomerically pure products. It is known that the retention times of hollow higher fullerenes increase as the cage size gets bigger (elution of C_{76} is followed by C_{78}, etc.; all discussions of the HPLC results in this work imply the use of Cosmosil Buckyprep column).[24] Endometallofullerenes, in general, and MNFs in particular, have longer retention times than hollow higher fullerenes with the same number of carbon atoms. This trend is followed by their trifluoromethylated derivatives as well. The $MNF(CF_3)_n$ compounds have longer retention times than hollow-$fullerene(CF_3)_n$ with the same n values, even when the size of a hollow fullerene is larger than the size of the MNF cage. For example, **Sc-2-1** has a significantly longer retention time (27 min) than $C_{60}(CF_3)_2$ (7.1 min; 100% toluene eluent at 5 mL/min flow rate), and **Sc-10-1** has a longer retention time than any isomer of $fullerene(CF_3)_{10}$ studied to date[25] (see Figure 1 and SI). The longer retention times of MNFs and their trifluoromethylated derivatives facilitate HPLC isolation of the isomerically pure $Sc_3N@(C_{80}\text{-}I_h)(CF_3)_n$ compounds. As shown in Figure 1, even with the use of pure toluene as the eluent, the range of retention times for the $Sc_3N@(C_{80}\text{-}I_h)\text{-}(CF_3)_{2-12}$ compounds is 6 times wider than that for $C_{60}\text{-}(CF_3)_{2-12}$.[25] As a result, only one stage of the HPLC separation (using toluene as an eluent) was sufficient for the isolation of six isomers of $Sc_3N@(C_{80}\text{-}I_h)(CF_3)_n$ (**Sc-2-1**, **Sc-4-1**, **Sc-4-2**, **Sc-8-1**, **Sc-8-2**, and **Sc-10-1**; see details in Figures SI-2−6 and the experimental section of the SI). The most abundant **Sc-2-1** and **Sc-10-1** isomers were isolated with 98+% purity (based on ^{19}F NMR spectroscopy and HPLC trace integration). The spectroscopic data for the purified fractions included mass spectra, one- and two-dimensional (1D and 2D) ^{19}F NMR spectra, and UV−vis spectra, which are given in SI (Figures SI-5−12).

The difference in solubility of the $Sc_3N@(C_{80}\text{-}I_h)(CF_3)_n$ compounds with different n values allowed us to further increase the efficiency of the HPLC separation. For example, using the three-solvent extraction procedure (see above) we easily isolated a fraction containing $Sc_3N@(C_{80}\text{-}I_h)(CF_3)_n$ compounds with $n > 10$. Then this hexane extract was subjected to a single-stage HPLC separation using weaker eluents (70/30 or 90/10 v/v heptane/toluene mixtures or even 100% heptanes); this procedure afforded a simple isolation of **Sc-16-1**, **Sc-16-2**, **Sc-14-1**, and **Sc-14-2**. The $Sc_3N@(C_{80}\text{-}I_h)(CF_3)_{12}$ isomers (**Sc-12-1**, **Sc-12-2**, **Sc-12-3**, and **Sc-12-4**) were purified using 30/70 toluene/heptane and 10/90 toluene/heptane eluents (Figure SI-2 [SI]). Without the initial selective extraction of highly trifluoromethylated MNFs, the use of the single-stage HPLC separation protocol, which employs a weak eluent, would be impractical.

Previously, the use of AgTFA for trifluoromethylation of hollow fullerenes was shown to result in the formation of numerous products including mixed trifluoromethylated/hydrogenated products (possibly due to the presence of traces of moisture in AgTFA).[26−28] These mixed trifluoromethylated/hydrogenated compounds made HPLC separation procedures significantly more complicated. In some cases, crude products were sublimed under vacuum at high temperature in order to remove hydrogenated byproducts prior to the HPLC separation.[26] To our surprise, such partially hydrogenated compounds were not observed at all in the products of $Sc_3N@(C_{80}\text{-}I_h)$/AgTFA reactions; therefore, no additional sublimation (which is known to drastically decrease the yields of trifluoromethylfullerenes (TMFs)[28]) was required for these crude products prior to HPLC separation.

2.2. Other Reactions. In this section, we describe preliminary results for various polyaddition reactions with $Sc_3N@(C_{80}\text{-}I_h)$, $Sc_3N@(C_{80}\text{-}I_h)(CF_3)_n$, and $Er_3N@(C_{80}\text{-}I_h)$. To explore the reactivity of $Sc_3N@(C_{80}\text{-}I_h)$ toward other radical additions (besides trifluoromethylation), we studied some halogenation reactions (fluorination and bromination) and perfluoroisopropylation reaction, for the first time. Using an MNF with a different cluster-forming metal, $Er_3N@(C_{80}\text{-}I_h)$, we studied trifluoromethylation and perfluoroisopropylation reactions. The reactivity of $Sc_3N@(C_{80}\text{-}I_h)(CF_3)_n$ was probed using radical benzylation and Bingel−Hirsch cyclopropanation reactions. These reactions were performed on a small scale of 1 mg (or less) of a fullerene substrate, so the overall amounts of the products were sufficient only for the mass spectrometric and HPLC analyses. Such choice of the reactions and analytical methods allowed us to obtain some initial data on the reactivity, i. e., to learn whether a certain reaction occurred at all; and, where it did form products, to determine effect of the substituent size on the maximal addition degrees to the MNF cages. The reaction conditions used previously for preparation of the corresponding hollow fullerene derivatives, were used as the starting points in derivatization of MNFs; thereby, a direct comparison of general reactivities of MNFs and hollow fullerenes was made possible.

2.2.1. Fluorination. The fluorine atom is the second smallest substituent (after the hydrogen atom), and it was expected that the maximum substitution degree can be achieved for fluorinated derivatives of $Sc_3N@(C_{80}\text{-}I_h)$, as has long been established for fluorinated hollow fullerenes.[29] In addition, fluorination is a highly thermodynamically favoured process as it results in the formation of the strong C(cage)−F bonds. From the wide variety of the fluorinating agents (FAs) that were used in the past for fluorination of fullerenes, we have chosen several transition metal fluorides, which are known to fluorinate hollow fullerenes with a high degree of selectivity.[30]

The fluorination of $Sc_3N@(C_{80}\text{-}I_h)$ was performed using K_2PtF_6, MnF_3, CoF_3, and $KMnF_4$ as fluorinating agents under dynamic vacuum at 380−550 °C for 2−6 h. The ratio of $Sc_3N@(C_{80}\text{-}I_h)$/FA was varied from 1:10 to 1:388 (see [SI]). Although similar reaction conditions resulted in the successful preparation of $C_{60(70)}F_n$ compounds,[30] formation of fluorinated $Sc_3N@(C_{80}\text{-}I_h)$ derivatives was not observed. Furthermore, no observable unreacted $Sc_3N@(C_{80}\text{-}I_h)$ could be detected after the reaction as well, which is indicative of its decomposition during the reaction.

In light of these findings we reacted a 1-mg sample of $Sc_3N@(C_{80}\text{-}I_h)$ with F_2 gas diluted with N_2 (20% F_2) using a flow-tube reactor. While slowly raising the temperature of the reactor, we allowed a flow of F_2/N_2 mixture to pass over the solid sample of $Sc_3N@(C_{80}\text{-}I_h)$. No changes were observed up to 250 °C, but a further increase in temperature (up to 300 °C) led to the degradation of the MNF substrate. It is notable that, unlike $Sc_3N@(C_{80}\text{-}I_h)$, hollow fullerenes readily undergo fluorination under these conditions to give highly fluorinated stable derivatives.

Our earlier unpublished data on the fluorination of a sample with unknown content of $Sc_3N@C_{80}$ were briefly communicated by others in ref 31. The evidence for the fluorination was based on the results of an in situ fluorination in a Knudsen cell-equipped mass spectrometer.[32] However, the resolution of that MS instrument was not sufficient for unambiguous ion identification: fluorinated hollow fullerenes could have been misidentified as ions due to $Sc_3N@C_{80}F_n$; therefore, that report on fluorinated $Sc_3N@C_{80}$[31] should be considered unreliable.

In conclusion, the behavior of $Sc_3N@C_{80}$ in fluorination reactions is very different from that of hollow fullerenes. None of the methods that were successfully used to fluorinate hollow fullerenes produced fluorinated products of $Sc_3N@C_{80}$. It appears that the cage degradation takes place during the attachment of F atoms to the $Sc_3N@C_{80}$ cage in all examined cases (see below). It is known from structural studies of hollow fluorofullerenes that extensive cage distortions occur upon fluorination, which are accompanied by a considerable (up to 20%) elongation of the cage C−C bonds.[33,34] One can speculate that these distortions may weaken the carbon cage of MNFs that bears multiple fluorine atoms, causing its complete destruction via cage opening.

Interestingly, the treatment of $Sc_3N@C_{80}$ with CF_3I at similar temperatures (see section above) did not cause any cage degradation, instead, we succeeded in the formation of $Sc_3N@C_{80}(CF_3)_n$. A seeming contradiction can be explained by the fact that attachment of CF_3 radicals to the $Sc_3N@C_{80}$ cage occurs mostly in the para or meta positions with respect to each other; therefore, the corresponding cage distortions are much smaller, and variation in C−C bond lengths as compared to those in underivatized molecules is smaller too (for example, the difference between the shortest and the longest bonds in **Sc-16-1** is only 13%).[16]

2.2.2. Perfluoroisopropylation of $Sc_3N@(C_{80}\text{-}I_h)$. Polyadditions of bulky $i\text{-}C_3F_7$ radicals to $Sc_3N@(C_{80}\text{-}I_h)$ are likely to yield derivatives with a smaller number of added groups and unprecedented addition patterns (as recently confirmed by the studies of $HF(i\text{-}C_3F_7)_n$ derivatives).[35] We carried out a photochemical reaction of $Sc_3N@(C_{80}\text{-}I_h)$ with $i\text{-}C_3F_7I$ in a sealed quartz ampule at room temperature for 47 h. The addition of up to 12 bulky $i\text{-}C_3F_7$ radicals per cage was observed (Figure SI-13 [SI]); in contrast, a trifluoromethylation reaction performed under similar conditions yielded $Sc_3N@(C_{80}\text{-}I_h)(CF_3)_n$ product with n_{max} = 18. A preliminary HPLC analysis indicated that isolation of the pure isomers of $Sc_3N@(C_{80}\text{-}I_h)(i\text{-}C_3F_7)_n$ from the crude product may be challenging because of the low retention times of highly substituted derivatives and also because of the presence of many isomers for specific compositions. The literature data on the photochemical reaction of $La@(C_{82}\text{-}C_s)$ with $C_8F_{17}I$ showed that at least seven isomers were formed even of the bis-derivative $La@(C_{82}\text{-}C_s)(C_8F_{17})_2$, which confirms that room-temperature polyadditions are typically highly nonselective.[36] More work is necessary in order to optimize the synthetic methods for the preparation of these potentially important MNF derivatives.

2.2.3. Reaction of $Sc_3N@(C_{80}\text{-}I_h)(CF_3)_{10}$ with $C_6H_5CH_2Br$. Previously, a 1-h photochemical reaction of $Sc_3N@(C_{80}\text{-}I_h)$ (or $Lu_3N@(C_{80}\text{-}I_h)$) with a large excess of $C_6H_5CH_2Br$ (1000 equiv) was reported to lead to the formation and isolation of derivatives with only two benzyl groups.[37] Such puzzling high selectivity suggested that we could use this reaction to explore the reactivity of trifluoromethylated $Sc_3N@(C_{80}\text{-}I_h)(CF_3)_n$ derivatives. At first, we performed a photochemical benzylation experiment with a hollow TMF, $C_1\text{-}C_{70}(CF_3)_{10}$. To our surprise, the reaction occurred readily, and addition of up to six benzyl groups was observed in the atmospheric pressure chemical ionization mass spectrum (APCI MS) of the crude product. Furthermore, only a limited number of isomers were formed in the reaction, which allowed facile isolation and initial spectroscopic characterization of several pure single isomers with 2, 4, and 6 benzyl groups (see Figure SI-14a−d [SI]). For this study, this experiment provided a solid proof that the presence of multiple electron-withdrawing CF_3 groups on the fullerene cage does not decrease its reactivity toward addition of benzyl radicals. Next, a photochemical reaction between **Sc-10-1** dissolved in 2 mL of deoxygenated toluene with an excess of benzyl bromide (16.8 equiv) was carried out in a quartz ampule at room temperature. After 1 h, the reaction solution changed color from green to dark brown. The HPLC analysis of the product showed no traces of unreacted starting material, whereas the short retention time of the main products indicated that multiple additions to **Sc-10-1** took place. This was confirmed by mass spectrometry; the NI APPI MS showed the presence of ions due to the addition of up to six benzyl groups to **Sc-10-1** (Figure 2). The peak assignments were confirmed by matching the theoretical and experimentally observed isotopic patterns of the corresponding peaks (Figure SI-14e [SI]). This result is in striking contrast with the above-mentioned data on the exceptionally high selectivity of the bis-addition of benzyl radicals to a bare cage of $Sc_3N@(C_{80}\text{-}I_h)$.[37]

Such high reactivity of trifluoromethylated $Sc_3N@(C_{80}\text{-}I_h)$ toward further multiple radical additions uncovered in these preliminary experiments may provide efficient routes for the design of new molecules and useful materials based on trifluoromethylated MNFs.

2.2.4. Bingel−Hirsch Reaction with $Sc_3N@(C_{80}\text{-}I_h)(CF_3)_{14}$. Initially we carried out a standard Bingel−Hirsch reaction[38−40] with underivatized $Sc_3N@(C_{80}\text{-}I_h)$. In agreement with the earlier report by Echegoyen et al.,[41] no reaction took place. Multiple repetitions of this reaction under the same or slightly modified conditions have not been successful either. However, when a sample of the crude mixture of isomers of $Sc_3N@(C_{80}\text{-}I_h)(CF_3)_{14}$ was used as a substrate for the same reaction, cycloaddition occurred almost instantaneously at room temperature. The NI MALDI mass spectrum of the obtained product demonstrated the selective addition of just one cycloadduct as shown

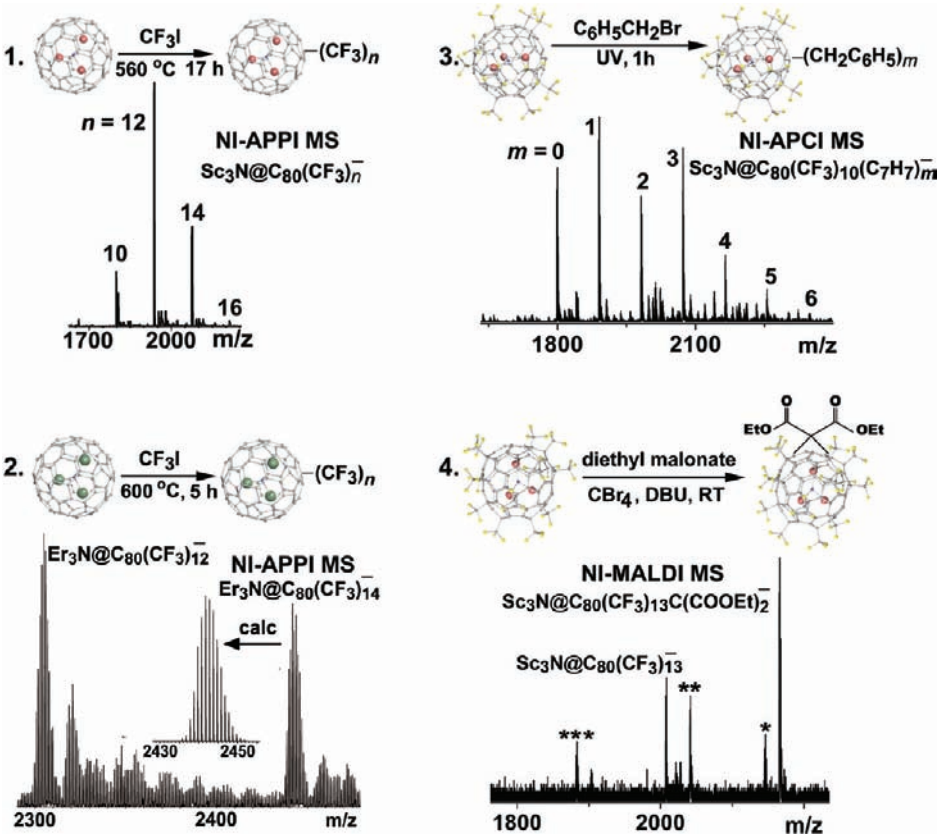

Figure 2. Mass spectra of the products of the following reactions: (1) NI APCI MS of the crude product of the reaction between $Sc_3N@(C_{80}\text{-}I_h)$ and CF_3I in the GTGS reactor; (2) NI APCI MS of the crude product of the reaction between $Erc_3N@(C_{80}\text{-}I_h)$ and CF_3I in the GTGS reactor; (3) NI APCI MS of the crude product of the photochemical reaction between $Sc_3N@(C_{80}\text{-}I_h)(CF_3)_{10}$ (**Sc-10-1**) and $C_6H_5CH_2Br$ in toluene solution; (4) NI MALDI MS of the crude product of the Bingel−Hirsch reaction with $Sc_3N@(C_{80}\text{-}I_h)(CF_3)_{10-14}$.

in Figure 2. The amount of the product was too small to study its isomeric composition and perform a detailed spectroscopic characterization. This result shows that $MNF(CF_3)_n$ compounds exhibit an unexpectedly high reactivity toward further derivatization. The fact that even derivatives with as many as 14 CF_3 groups on the cage undergo monocycloaddition readily, in contrast to the underivatized MNFs, provides a showcase for new and versatile routes for further MNF functionalization.

2.2.5. Trifluoromethylation of $Er_3N@(C_{80}\text{-}I_h)$. Two experiments were performed with the $Er_3N@C_{80}$ samples. In the first experiment, a partially purified sample of $Er_3N@C_{80}$ that contained a mixture of both I_h and D_{5h} isomers and some $Er_2@C_{2n}$, was used for the reaction with CF_3I in a sealed glass ampule at 432 °C for 48 h. To our surprise, the PI EI MS analysis of the product showed that only trifluoromethylation of the minor components in the starting material had occurred giving rise to the following peaks in the mass spectra: $Er_2@C_{88}(CF_3)_{15}^+$, $Er_2@C_{88}(CF_3)_{17}^+$, $Er_2@C_{84}(CF_3)_{19}^+$, $Er_2@C_{88}(CF_3)_{19}^+$, and $Er_2@C_{90}(CF_3)_{19}^+$. Although these experimental conditions appeared unsuitable for trifluoromethylation of the MNF $Er_3N@C_{80}$, the result shows that this method is useful for the perfluoroalkylations of mono- and dimetallic EMFs.

The reaction of purified $Er_3N@(C_{80}\text{-}I_h)$ with CF_3I was carried out at 500 °C for 5 h in the gradient-temperature gas−solid reactor.[42] This reaction showed excellent conversion and led to the synthesis of $Er_3N@(C_{80}\text{-}I_h)(CF_3)_n$ compounds with n = 12−14 according to the NI APPI MS analysis (Figure 2). The same degree of trifluoromethylation was observed for $Sc_3N@(C_{80}\text{-}I_h)$ when the reaction was performed under similar experimental conditions. We may now conclude that no differences were observed in the reactivity (and the degree of trifluoromethylation) of these two MNFs. We demonstrated earlier that the high temperature perfluoroalkylation works similarly well for both isomers of $Sc_3N@C_{80}$ (of D_{5h} and I_h symmetries).[18] Taking into account our results on the trifluoromethylation of $Er_3N@(C_{80}\text{-}I_h)$, we can extend this statement to say that high-temperature perfluoroalkylation may work indiscriminately well for cluster and cage sizes of MNFs, including the ones that were found to be relatively inert in many other organic functionalizations (e.g., $Sc_3N@(C_{80}\text{-}I_h)$).

2.3. Molecular Structures and Addition Patterns. *2.3.1. General Remarks.* Single-crystal X-ray diffraction is the most informative technique for the determination of molecular structures of fullerenes and their derivatives. A considerable success has been achieved to date in the X-ray studies of perfluoroalkylfullerene (PFAFs): structures of nearly 100 compounds were determined,[22] including the structures of perfluoroalkylated MNFs (**Sc-14-1** and **Sc-16-1**,[16] and two new structures are reported here for the first time: **Sc-10-1** and **Sc-12-1** (see below)). Importantly, this technique is nondestructive and requires very small amounts of compounds. Furthermore, the use of a high-intensity synchrotron source allows measurements on a single crystal of a size of tens-to-a hundred micrometers in all dimensions. However, growing high-quality single crystals is oftentimes a challenging task; other potential problems include different types of disorder in the crystals. Therefore, other

methods have to be applied for the structural studies; e.g., we showed recently that the combination of ^{19}F NMR spectroscopy and DFT calculations represents a powerful structural tool for TMFs of hollow fullerenes. The molecular structural data obtained using this approach were shown to be (almost) as reliable as single-crystal X-ray analysis.[24,25,43,44]

Typically, a solution ^{19}F NMR spectrum is used to evaluate the symmetry and the addition pattern of CF_3 groups using chemical shifts, through-space coupling constants (J_{FF} values), splitting patterns of the peaks, and correlational spectroscopy data (^{19}F COSY NMR). On the basis of the large number of single-crystal X-ray structures of various TMFs, it is now known that CF_3 groups tend to form "ribbons" due to their addition to the adjacent hexagons (rarely to pentagons) of a fullerene cage. Because of the steric requirement of bulky CF_3 groups, they rarely occupy vicinal ("ortho") positions. The only known examples of fullerene$(CF_3)_{n\leq 12}$ are C_s-$C_{60}(CF_3)_6$[45] and C_{2h}-$C_{60}(CF_3)_{12}$[25] (the formation of stable skew-pentagonal pyramid addition patterns is a likely driving force behind the formation of these compounds); for higher-substituted fullerene$(CF_3)_{n>14}$ the addition of CF_3 groups to ortho positions was observed more frequently (e.g., $C_{60}(CF_3)_{16}$,[46] $C_{70}(CF_3)_{16}$,[47] and $C_{70}(CF_3)_{18}$[47]). Trifluoromethyl groups tend to add to meta (m) and para (p) positions of the fullerene hexagons. Sometimes CF_3 groups form isolated pairs of para-substituted hexagons; the examples of such compounds are p-$C_{60}(CF_3)_2$, p-$C_{70}(CF_3)_2$ (**60-2-1** and **70-2-1**, both compounds were prepared as single isomers), and p,p-$C_{60}(CF_3)_4$ (**60-4-3**). As mentioned above, the formation of a ribbon of CF_3-substituted hexagons is more typical for hollow fullerenes (e.g., pmp-$C_{60}(CF_3)_4$ or p^3mp-$C_{60}(CF_3)_6$, **60-4-1** or **60-6-1**). When CF_3 groups are located on the same hexagon or a pentagon, they are sufficiently close to interact through space via the overlap of lone p-orbitals of the fluorine atoms (Fermi coupling) which gives rise to J_{FF} coupling constants of 0−25 Hz (depending on the bond distances and angles, see ref 25). For example, an isolated pair of p-CF_3 groups gives rise to two quartets with J = 16−20 Hz if the chemical shifts corresponding to the signals of the CF_3 groups are different; if chemical shifts are isochronous, then the through-space J splitting is nonobservable, and peaks collapse into a single line (e.g., $C_{60}(CF_3)_2$; the same effect is responsible for the lack of observable through-bond J_{F-F} splitting for the germinal fluorines of rapidly rotating CF_3 groups). A trifluoromethyl group that terminates a ribbon of $C_6(CF_3)_2$ hexagons also manifests itself as a quartet peak in the ^{19}F NMR spectrum; the "internal" CF_3 groups that interact with two CF_3 neighbors typically show up as apparent septets (if the corresponding through-space J_{FF} constants are similar). The detailed discussion of the ^{19}F NMR analysis of the addition patterns of TMFs goes beyond the scope of this paper and can be found elsewhere;[25] it sufficies to say that this information can be used to identify a particular isomer of the TMF in question or to lower the number of possible isomers from billions to several thousand or less. If many isomers satisfy the restrictions of the ^{19}F NMR spectrum, then their relative stability can be calculated, and the most stable structure(s) can be assumed to correspond to the experimentally observed ones. This assumption of at least partial thermodynamic control over the selectivity of the high-temperature trifluoromethylation was confirmed experimentally; the TMFs prepared by high-temperature methods have structures that were among the most stable ones (usually within 10−15 kJ/mol, with only a few exceptions[48]). Typically AM1 calculations are used to quickly identify the most stable structures and calculate their approximate geometry; then DFT calculations are used for final structure optimization and enthalpy calculation. Such an approach was shown to be highly reliable for many trifluoromethylated derivatives of hollow fullerenes.[24,25,43,44] It is assumed that the rules governing CF_3 addition to $Sc_3N@C_{80}$ may be similar to the ones established for the trifluoromethylation of hollow fullerenes (e.g., ribbons of p- and m-$C_6(CF_3)_2$ hexagons as the main addition motif). The recently reported single-crystal X-ray structures of **Sc-16-1** and **Sc-14-1** confirm this suggestion.[16] It is notable that besides the formation of the predicted ribbons of p/m-$C_6(CF_3)_2$ hexagons these two isomers also featured the addition of CF_3 groups to the triple-hexagon junctions (THJ) of the cage, which have not been observed for the TMFs of the hollow higher fullerenes[25,43,44] (this difference in the chemical behavior of $Sc_3N@C_{80}$ may be due to the formal 6-fold electron transfer from the nitride cluster to the carbon cage). Therefore, theoretical and experimental studies of $Sc_3N@C_{80}(CF_3)_n$ isomers have to account for the possible structures that were ruled out as unlikely for the TMFs of hollow fullerenes. Furthermore, fast semiempirical AM1 (or PM3) method cannot be used for Sc-containing compounds; more computationally intensive DFT methods have to be used which limits the number of $Sc_3N@C_{80}(CF_3)_n$ structures that can be surveyed. Finally, as we have shown in our earlier work for $Sc_3N@C_{80}(CF_3)_2$,[17] the relative energies of the isomers with the same CF_3 addition pattern but different position of the Sc_3N cluster inside the cage can differ by as much as 60 kJ/mol (in contrast, for the underivatized $Sc_3N@C_{80}$ the difference between different orientations of the Sc_3N cluster inside the cage is much smaller, in the range of 10 kJ/mol). Hence, for each isomer of $Sc_3N@C_{80}(CF_3)_n$ several conformers with different positions of Sc_3N cluster should be considered, and this stage of computations cannot be fully automated. In our recent extensive study of the possible isomers of $M_3N@C_{68+x}$ (x = 0−20), we showed that the carbon cage isomerism in MNFs is determined by two major factors: (i) the stability of a given cage isomer in the (6−) state and (ii) the fullerene "form factor" representing the size and shape of the carbon cage should match the shape of the cluster.[49] Those studies demonstrated that when C_{68+x}^{6-} cages are unstable, then such $M_3N@C_{68+x}$ (x = 0−20) are not formed at all or become non-IPR (e.g., $Sc_3N@C_{72}$ or $Sc_3N@C_{74}$). As the initial hypothesis for this work, we suggest that the same rules may be applicable to the derivatives of $Sc_3N@C_{80}$. These modified rules can be formulated as follows: the stable isomers of $Sc_3N@C_{80}(CF_3)_n$ (i) are based on the most stable isomers of $C_{80}(CF_3)_n^{6-}$ and (ii) have suitable arrangement of CF_3 groups so that effective coordination of Sc_3N to the cage can be realized. Therefore the search of the lowest energy isomers of $Sc_3N@C_{80}(CF_3)_n$ was performed in two steps: (i) the most stable $C_{80}(CF_3)_n^{6-}$ isomers were identified, followed by (ii) the studies of $Sc_3N@C_{80}(CF_3)_n$ isomers with the same CF_3 addition patterns. All these factors make theoretical studies of $Sc_3N@C_{80}(CF_3)_n$ compounds significantly more computationally and labor intensive then the analogous studies of TMFs of hollow fullerenes.

2.3.2. Fluorine-19 NMR Spectra and DFT-Assisted Elucidation of Addition Patterns

2.3.2.1. $Sc_3N@C_{80}(CF_3)_2$. Earlier, we reported that ^{19}F NMR spectrum of $Sc_3N@C_{80}(CF_3)_2$ consists of a single line at −71.4 ppm in $CDCl_3$ solvent (relative to −164.9 ppm chemical shift of C_6F_6 internal standard).[18] This indicates that the two CF_3 groups are symmetry related and therefore isochronous, and on the basis

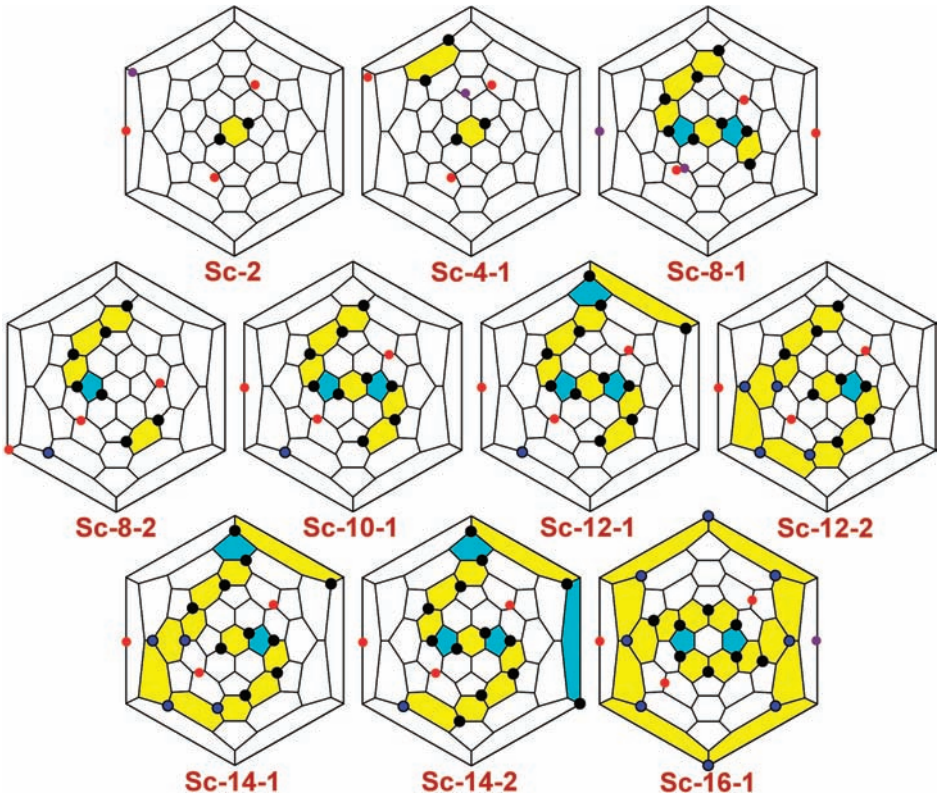

Figure 3. Schlegel diagrams of $Sc_3N@(C_{80}\text{-}I_h)(CF_3)_n$ derivatives with the determined addition patterns. Black dots denote CF_3-bearing carbon atoms, black dots with blue centers denote the CF_3-bearing THJs. Red dots schematically denote position of Sc atoms; when two conformers with close energies are possible, positions of Sc atoms in the higher-energy structure are denoted by violet dots.

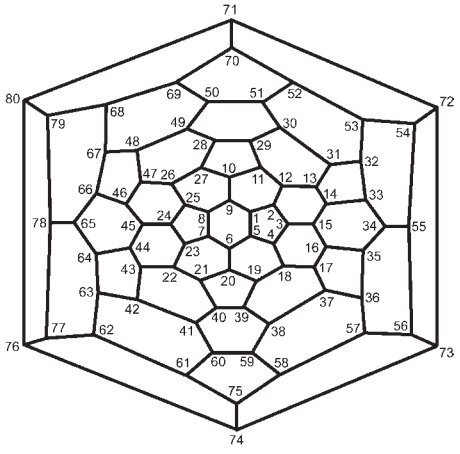

Figure 4. Schlegel diagram of $Sc_3N@(C_{80}\text{-}I_h)$ with IUPAC numbering.

of the analogy with the CF_3 derivatives of the hollow fullerenes, we have suggested the isomeric structure with the *p*-$C_6(CF_3)_2$ hexagon shown in Figure 3 (1,7-isomer in IUPAC nomenclature, see Figure 4 for the Schlegel diagram with the atom numbering).

In this work we report an extended survey of the possible isomers of $C_{80}(CF_3)_2^{6-}$ and corresponding $Sc_3N@C_{80}(CF_3)_2$ to support our earlier structural conjecture.[18] Calculations of all 40 possible isomers of $C_{80}(CF_3)_2^{6-}$ (for I_h-C_{80} cage) have shown that 1,7-isomer is indeed the most thermodynamically stable structure; its HOMO−LUMO gap was calculated to be 1.21 eV. The vicinal isomer 1,2-$C_{80}(CF_3)_2^{6-}$ with CF_3 groups attached to the adjacent carbon atoms was found to be the second most stable structure with the relative energy of 24.4 kJ/mol and the HOMO−LUMO gap of 1.22 eV. Surprisingly, the third most stable isomer is 6,9-$C_{80}(CF_3)_2^{6-}$ with two CF_3 groups attached to the triple-hexagon junctions (THJs). Note that for the zero-charged hollow fullerenes, addition of CF_3 groups to THJs is known to be energetically very unfavorable (e.g., the isomers of $(C_{78}\text{-}C_{2v}(3))(CF_3)_2$ with one or both CF_3 groups attached to the THJ(s) are at least 70 kJ/mol less stable than the most stable isomer of $(C_{78}\text{-}C_{2v}(3))(CF_3)_2$).[24] All other isomers of $C_{80}(CF_3)_2^{6-}$ are at least 30 kJ/mol higher in energy. They also have much smaller HOMO−LUMO gaps (less than 1 eV). The isomer 1,9-$C_{80}(CF_3)_2^{6-}$ which has one of the CF_3 groups attached to THJ, is one of the least stable isomers (ΔE = 67.5 kJ/mol), however, it has a relatively high HOMO−LUMO gap of 1.19 eV.

The simulation of the most likely $Sc_3N@C_{80}(CF_3)_2$ isomers (selected using the criteria outlined above) showed that 1,7-isomer has the lowest energy and the highest HOMO−LUMO gap of 1.15 eV; this confirms our original conjecture.[18] Importantly, the vis−NIR absorption spectrum of $Sc_3N@C_{80}(CF_3)_2$ is very similar to the spectra of the bis-silyl derivative $Sc_3N@C_{80}((Mes_2Si)_2CH_2)$[50] and bis-benzyl derivative $Sc_3N@C_{80}(CH_2C_6H_5)_2$,[37] (both were found to be 1,7-isomers of $Sc_3N@C_{80}$ by single-crystal X-ray diffraction). We found that the second most stable isomer is 1,2-$Sc_3N@C_{80}(CF_3)_2$ with ΔE = 32.5 kJ/mol and the HOMO−LUMO gap of 1.05 eV.

The exhaustive calculations of the conformers of the 1,7-$Sc_3N@C_{80}(CF_3)_2$ with different orientations of the Sc_3N cluster with respect to the *p*-$C_6(CF_3)_2$ hexagon were also carried out. They gave the lowest energy for a conformer with Sc atoms

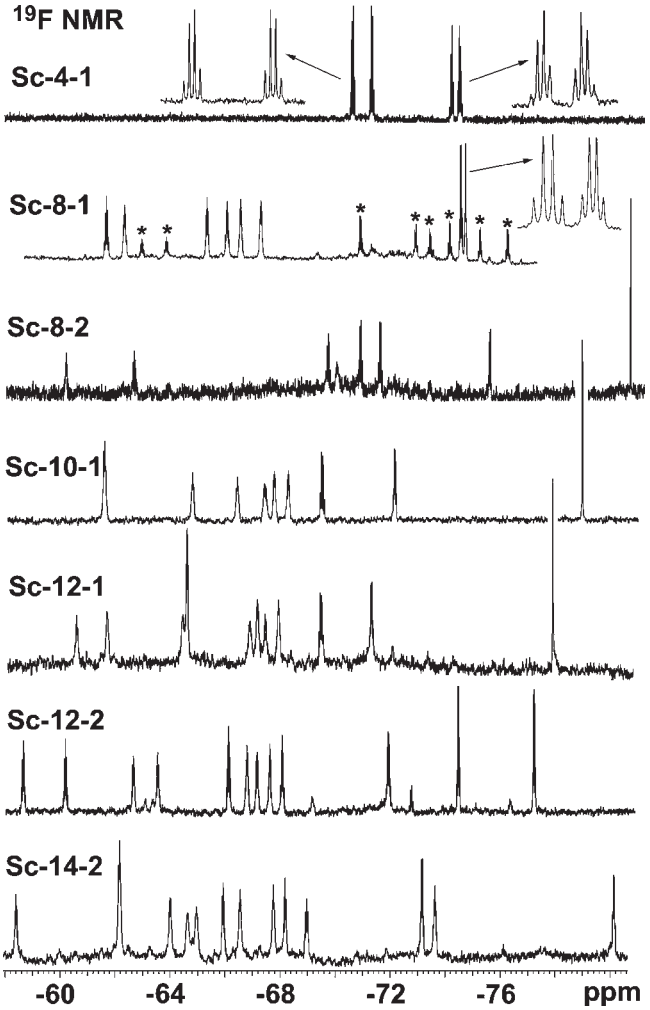

Figure 5. The ^{19}F NMR spectra (376.48 MHz, $CDCl_3$, C_6F_6 internal standard) of the purified isomers of $Sc_3N@(C_{80}\text{-}I_h)(CF_3)_n$.

coordinated to the sp^2 cage carbons that are para to the sp^3-$C(CF_3)$ carbons. The conformers with Sc atoms coordinated directly to the sp^3-$C(CF_3)$ atoms were found to have the highest energy (i.e., lowest stability).

2.3.2.2. $Sc_3N@C_{80}(CF_3)_4$. Fluorine-19 NMR spectrum of $Sc_3N@C_{80}(CF_3)_4$ showed four equal-intensity quartets (see Figure 5). This indicates that this C_1-symmetric compound has two isolated pairs of interacting CF_3 groups that give rise to the observed splitting pattern; the pairs of interacting CF_3 groups have to share the same hexagon or pentagon in order for the through-space spin−spin coupling to be possible. Contrary to the previously discussed case of $C_{80}(CF_3)_2^{6-}$, the calculations of all 90 isomers of $C_{80}(CF_3)_4^{6-}$ with two pairs of CF_3 groups on nonadjacent pentagons or hexagons did not reveal an especially favorable structure. The relative energies of these isomers are distributed fairly uniformly in the range of 0−90 kJ/mol with the frequency of approximately one isomer per kJ/mol; several low energy isomers have also relatively large HOMO−LUMO gaps of over 1.0 eV. The calculations of $Sc_3N@C_{80}(CF_3)_4$ isomers performed for 15 different addition patterns of $C_{80}(CF_3)_4^{6-}$ that were found to have the lowest energy and/or large HOMO−LUMO gaps showed that these endohedral fullerene derivatives have a broader spread of relative energies. Calculations revealed that there are three isomers of $Sc_3N@C_{80}(CF_3)_4$ within a 10 kJ/mol range; one of them has C_s symmetry, and the other two are nonsymmetric. The lowest-energy C_s-isomer (1,7,31,52-$Sc_3N@C_{80}(CF_3)_4$) was found to have a relatively small HOMO−LUMO gap of 0.94 eV; a virtually isoenergetic C_1-1,7,32,51-$Sc_3N@C_{80}(CF_3)_4$ has a HOMO−LUMO gap of 1.10 eV which is the highest among the lowest energy isomers. C_2-1,7,52,72-$Sc_3N@C_{80}(CF_3)_4$ was found to have a HOMO−LUMO gap of 1.12 eV, but it is 14.3 kJ/mol less stable. On the basis of its low relative energy, a large HOMO−LUMO gap, and C_1 symmetry, we propose that the experimentally observed isomer of $Sc_3N@C_{80}(CF_3)_4$ has *p,p*-1,7,32,51 addition pattern. The two other most stable C_1 isomers are 1,7,54,70-$Sc_3N@C_{80}(CF_3)_4$ (ΔE = 8.5 kJ/mol, gap = 0.99 eV) and 1,7,14,35-$Sc_3N@C_{80}(CF_3)_4$ (ΔE = 14.4 kJ/mol, gap 0.96 eV). The isomers with low relative energies and narrow gaps (below 1.0 eV) may also be produced during the reaction, but they are more reactive (due to narrow gaps) and therefore they are likely to be rapidly converted to the products with the larger number of CF_3 groups. Note that the HOMO−LUMO gap of the proposed $Sc_3N@C_{80}(CF_3)_4$ isomer is 0.1 eV smaller than that gap of $Sc_3N@C_{80}(CF_3)_2$, which is in agreement with the experimental vis−NIR spectra of these two compounds (Figure 10).

2.3.2.3. $Sc_3N@C_{80}(CF_3)_8$-1. Fluorine-19 NMR spectrum of **Sc-8-1** showed eight equal intensity peaks, two of which were quartets and six others were multiplets (Figure 5). On the basis of the principles outlined above, the addition pattern of **Sc-8-1** is found to consist of a ribbon of seven edge-sharing $C_6(CF_3)_2$ and/or $C_5(CF_3)_2$ units. Though this restricts the number of possible structures of **Sc-8-1** (only the isomers with a ribbon of CF_3 groups should be considered), this number is still very large (tens of thousands). Therefore the computations were performed in several steps. At the first stage we have performed AM1 point energy calculations of all possible ribbon isomers of $C_{80}H_8^{6-}$ (excluding the ones with vicinal substituents). The isomers of $C_{80}H_8^{6-}$ were then sorted according to their energy; then the AM1 computations of the corresponding isomers of $C_{80}(CF_3)_8^{6-}$ were performed with the full optimization (starting from the most stable isomers of $C_{80}H_8^{6-}$). For these most stable isomers the point energy DFT/AM1 calculations were performed to reveal the most stable structures with the largest HOMO−LUMO gaps. When the most stable isomers of $C_{80}(CF_3)_8^{6-}$ were found, we could do the calculations with Sc_3N cluster placed inside the carbon cage. Since relative energies of the $Sc_3N@C_{80}(CF_3)_n$ isomers can dramatically depend on the position of the Sc_3N cluster, we had to perform several calculations for each isomer of $Sc_3N@C_{80}(CF_3)_n$ corresponding to the different orientations of the Sc_3N cluster inside the cage. First, a screening of possible $Sc_3N@C_{80}(CF_3)_n$ isomers using a less computationally intensive DFT-based tight-binding approach (DFTB)[51−53] was performed. Then, full DFT PBE/TZ2P optimizations were performed for most stable structures (see SI for more details of multistep calculations). This final stage of the calculations showed that one particular addition pattern was much more stable then the alternatives, the most probable structure of **Sc-8-1.** This structure has two conformers with slightly different positions of Sc_3N cluster (they are different in energy by only 2.8 kJ/mol), and it is 38 kJ/mol more stable than any other isomer with a different addition pattern (the Schlegel diagrams for both conformers are shown in Figure 3). A peculiarity of this isomer is that the ribbon of the edge-sharing $C_6(CF_3)_2$ hexagons forms two semi-isolated benzenoid rings with Sc atoms coordinated to the cage in the close proximity to

the carbon atoms that would be sp^3 hybridized if the rings were fully isolated.

2.3.2.4. $Sc_3N@C_{80}(CF_3)_{10}$-1. One singlet, two quartets, and seven multiplets in the ^{19}F NMR spectrum of $Sc_3N@C_{80}(CF_3)_{10}$-1 (**Sc-10-1**) suggest that the addition pattern of this compound has a ribbon of nine CF_3 groups and a single isolated CF_3 group ("9 + 1" hereafter). The presence of the ribbon of nine CF_3 groups was also confirmed by the 2D ^{19}F COSY NMR spectroscopy (see Figure SI-7, SI). An extensive search for the possible structures with (9 + 1) addition motif was carried out. We assumed that the most stable (9 + 1) isomers of $C_{80}H_{10}^{6-}$ should be based on the stable ribbon isomers of $C_{80}H_8^{6-}$ (they should include them as substructures). The isomers of $C_{80}H_8^{6-}$ were sorted by the energy using AM1 point energy calculations. Then for each isomer of $C_{80}H_8^{6-}$ all possible $C_{80}H_{10}^{6-}$ isomers with (9 + 1) addition pattern were generated (each ribbon isomer of $C_{80}H_8^{6-}$ produces 50−60 isomers of $C_{80}H_{10}^{6-}$ with (9 + 1) addition pattern). The point energy AM1 calculations were continued until all newly generated isomers of $C_{80}H_{10}^{6-}$ with energies under 50 kJ/mol were identified. Then, the sequence of calculations analogous to the one described above for the case of $Sc_3N@C_{80}(CF_3)_8$ was carried out. As in the case of $Sc_3N@C_{80}(CF_3)_8$, we found one isomer of $Sc_3N@C_{80}(CF_3)_{10}$ (Schlegel diagram is shown in Figure 3) to be particularly stable; it is 40 kJ/mol more stable than all other isomers that were tested at the DFT level. Importantly, it turned out that this isomer is closely related to the most stable ribbon isomer of $Sc_3N@C_{80}(CF_3)_8$ (assigned to **Sc-8-1**); it can be obtained from it by a simple addition of two CF_3 groups without any additional rearrangement. The close similarity of these compounds is also apparent from their ^{19}F NMR spectra (see Figure 5). After this computational study was complete, we were able to confirm its predictions by the unambiguous single-crystal X-ray structure determination of $Sc_3N@C_{80}(CF_3)_{10}$-1 (**Sc-10-1**, see below).

An unusual feature of the proposed addition pattern of **Sc-10-1** is that one CF_3 group is attached to a triple hexagon junction (THJ) which has never been observed before for fullerene-$(CF_3)_n$ ($n \leq 16$) compounds. The addition to THJ was reported earlier for cycloadditions to $M_3N@C_{80}$.[54,55] It is notable that the CF_3 group attached to the THJ in **Sc-10-1** is "isolated", i.e., there are no other CF_3 groups attached to the shared hexagons. Due to the lack of through-space spin−spin coupling with the other CF_3 groups, this isolated CF_3 group gives rise to a singlet in the ^{19}F NMR spectrum (Figure 5). Earlier, using a large set of ^{19}F NMR measurements, we showed that the chemical shifts of CF_3 groups of $C_{60+x}(CF_3)_n$ derivatives are correlated with the geometry of the most stable conformer of the corresponding TMF (established by DFT calculations).[24,56] We found that CF_3 groups with the least eclipsed geometry (have the largest C−C−C−F torsion angles, see refs 24 and 56 for a detailed discussion) have the largest observed chemical shift values of negative 70−73 ppm. Typically these least eclipsed CF_3 groups occupy the least sterically hindered positions at the terminals of the CF_3-ribbon (and/or they make isolated *p*-$C_6(CF_3)_2$ moieties). Currently only one $C_{60+x}(CF_3)_n$ derivative with an isolated CF_3 group is known; it is $C_{70}(CF_3)_{10}$-5 isomer and its isolated CF_3 group has a chemical shift of −74.3 ppm. This is the largest chemical shift of all the $C_{60+x}(CF_3)_n$ derivatives studied up to date (this comprises over 60 different TMFs).[24,25,43,56] In this respect, the chemical shift of −78.9 ppm observed for the singlet in the ^{19}F NMR of **Sc-10-1** is still unusually large. We propose that such a large chemical shift is a fingerprint of the CF_3 group attached to a triple-hexagon junction (THJ).

2.3.2.5. $Sc_3N@C_{80}(CF_3)_{12}$-1. Exhaustive calculations for the isomers of $Sc_3N@C_{80}(CF_3)_n$ with $n > 10$ were found impractical due to (i) a dramatic increase of the number of possible isomers and (ii) a possibility to narrow down the search using the apparent similarities between the ^{19}F NMR spectra of various $Sc_3N@C_{80}(CF_3)_n$. We used this approach to generate a considerably smaller and therefore manageable set of candidate addition patterns of $Sc_3N@C_{80}(CF_3)_{12}$; this set was used as a starting point for the following calculations (the same approach was used for other $Sc_3N@C_{80}(CF_3)_n$ compounds as well, see below).

The ^{19}F NMR spectrum of **Sc-12-1** with one singlet, two quartets, and nine multiplets indicates that this compound has the (11 + 1) addition pattern. On the basis of the similarities of the ^{19}F NMR spectra of **Sc-12-1** and **Sc-10-1**, we have assumed that (i) the isolated CF_3 group is attached to a THJ since its chemical shift is −78.0 ppm and that (ii) an addition pattern of **Sc-12-1** can be obtained from the addition pattern of **Sc-10-1** by addition of a pair of CF_3 groups to one terminal of the ribbon of nine CF_3 groups, or by addition of one CF_3 group to each terminal of the ribbon. There are 23 isomers that satisfy these requirements; nine of them have one CF_3 group attached to a THJ as a part of the ribbon (in addition to the isolated CF_3 group). The lowest-energy structure was found to be 26 kJ/mol more stable than the second most stable isomer. It has also a large HOMO−LUMO gap of 1.24 eV. We assigned this most stable structure to **Sc-12-1** (Figure 3; **Sc-12-1** can be obtained from **Sc-10-1** by the addition of a pair of CF_3 groups to C54 and C70). Later this assignment was confirmed by a single-crystal X-ray diffraction study of **Sc-12-1** (see below).

Importantly, addition patterns of two $Sc_3N@C_{80}(CF_3)_n$ derivatives (**Sc-10-1** and **Sc-12-1**) have been first proposed on the basis of the ^{19}F NMR spectra and the computational study, and afterward the single-crystal X-ray determinations of their structures were carried out. These two independent validations of the approach developed by us for predictions of the addition patterns in trifluoromethylated hollow fullerenes are even more compelling as they were applied to much more complex molecular systems than the derivatized hollow fullerenes. With this convincing record in mind, we also proposed addition patterns of other $Sc_3N@C_{80}(CF_3)_n$ derivatives, whose single-crystal X-ray studies are not yet available.

2.3.2.6. $Sc_3N@C_{80}(CF_3)_{14}$-2. Fluorine-19 NMR spectrum of **Sc-14-2** showed 2 quartets and 12 multiplets (Figure 5) and the corresponding 2D ^{19}F COSY NMR spectrum revealed the connectivity of the CF_3 groups (Figure SI-8, SI). This evidence indicated that the addition pattern of **Sc-14-2** consists of a single ribbon of 14 CF_3 groups. Note that the position of the strongly shifted peak at −80 ppm is similar to the peaks due to the isolated CF_3 groups in the spectra of **Sc-10-1** and **Sc-12-1**, however for **Sc-14-2** this peak is split into a quartet. This indicates that a THJ-bonded CF_3 group is also present in **Sc-14-2** as one of the terminal groups. Since there are no other strongly shifted signals, we suggest that there are no other THJ-bonded CF_3 groups in the structure of **Sc-14-2**.

We assumed that the addition pattern of **Sc-14-2** results from the addition of four CF_3 groups to **Sc-10-1**, analogously to the cases described above. One group is added to the meta or para position in the THJ−CF_3 containing hexagon, so that this THJ-bonded CF_3 group becomes a terminal group of the ribbon. Three other groups should be added to the opposite terminal resulting in the ribbon of 14 CF_3 groups. Over one hundred

possible isomers satisfy these requirements. All of them were studied at the DFT level. The isomer shown in Figure 3 was found to have the lowest energy (at least 40 kJ/mol more stable than all other isomers) and the largest HOMO−LUMO gap of 1.36 eV. This structure is only 4 kJ/mol less stable than the recently reported **Sc-14-1** isomer (the DFT-predicted HOMO−LUMO gap of **Sc-14-1** is 1.415 eV). Based on the high stability and the large gap of this structure, we propose that this is the most probable addition pattern of **Sc-14-2**.

2.3.2.7. $Sc_3N@C_{80}(CF_3)_8$-2. Fluorine-19 NMR spectrum of $Sc_3N@C_{80}(CF_3)_8$-2 (**Sc-8-2**) indicated that this compound has one isolated CF_3 group and two ribbons formed by the remaining seven CF_3 groups; this implies either (5 + 2) or (4 + 3) ribbons (see Figure 5). On the basis of the similarities between the ^{19}F NMR spectra of **Sc-8-2** and **Sc-10-1**, we assumed that (i) the isolated CF_3 group is added to THJ since its chemical shift is −80.9 ppm; and that (ii) the addition pattern of **Sc-8-2** can be obtained from the addition pattern of **Sc-10-1** by the removal of two CF_3 groups. These two assumptions gave six (4 + 3 + 1) and six (5 + 2 + 1) possible isomers of **Sc-8-2** which were studied at the DFT level. Among these structures the (5 + 2 + 1) isomer shown in Figure 3 was found to have a HOMO−LUMO gap of 1.15 eV; furthermore it is 13.5 kJ/mol more stable than the proposed structure of **Sc-8-1**. The other isomers have smaller HOMO−LUMO gaps (1.00 eV or below) and are less stable by at least 22 kJ/mol. We also checked if stable addition patterns for **Sc-8-2** can be obtained by the removal of four CF_3 groups from **Sc-12-1** but no other stable isomers were found.

2.3.2.8. $Sc_3N@C_{80}(CF_3)_{12}$-2. Fluorine-19 NMR spectrum of **Sc-12-2** showed two quartets and 10 multiplets (see Figure 5); a corresponding 2D ^{19}F COSY NMR spectrum was also acquired (see Figure SI-9, SI). This evidence indicated that the addition pattern of **Sc-12-2** consists of the ribbon of 12 CF_3 groups. We analyzed all possible isomers of **Sc-12-2** formed by the removal of two CF_3 groups from either **Sc-14-1** or **Sc-14-2**. The lowest-energy structure that was found in this way is 16 kJ/mol less stable than **Sc-12-1** and has a large HOMO−LUMO gap of 1.24 eV. This isomer is based on the X-ray determined addition pattern of **Sc-14-1**; the lowest-energy isomer based on **Sc-14-2** is 28.2 kJ/mol less stable, and it has the gap of only 0.95 eV. On the basis of these results we propose that the stable structure might describe the **Sc-12-2** isomer (see Figure 3).

2.3.3. General Motifs of Addition Patterns of Trifluoromethylated Fullerenes. The determination of the addition pattern for a series of $Sc_3N@C_{80}(CF_3)_{2-16}$ (or at least an elucidation with a high degree of certainty) achieved in this work allowed us to formulate several general principles of multiple additions of CF_3 groups to $Sc_3N@C_{80}$ and hollow fullerenes (see refs 25 and 57 for the original formulations of such principles for hollow fullerenes). We present these principles below.

1 The structures of TMFs tend to be based on ribbons of edge-sharing $C_6(CF_3)_2$ hexagons (although such ribbons are not mandatory). In case of $Sc_3N@C_{80}$ cage these ribbons may also include $C_5(CF_3)_2$ pentagons (we found this to be common for $Sc_3N@C_{80}(CF_3)_{n\geq 8}$, e.g., **Sc-10-1**, **Sc-12-1**, **Sc-14-1**, and **Sc-16-1**). This differs from the behavior of trifluoromethylated hollow fullerenes where formation of $C_5(CF_3)_2$ pentagons is usually avoided (at least for the fullerene$(CF_3)_n$ with $n \leq 12$).
2 "Isolated" CF_3 groups are very rare for trifluoromethylated hollow fullerenes (only one such structure is known; it is a minor isomer of $C_{70}(CF_3)_{10}$, **70-10-5**[43]). In contrast, such isolated CF_3 groups were found to be common for $Sc_3N@C_{80}(CF_3)_n$ compounds, e.g., for the major isomers of $Sc_3N@C_{80}(CF_3)_n$ with n = 8, 10, and 12 (**Sc-8-2**, **Sc-10-1**, and **Sc-12-1**). Several other $Sc_3N@C_{80}(CF_3)_n$ compounds with the isolated CF_3 groups (according to ^{19}F NMR spectroscopy) have also been isolated, but the details of their structures are currently unknown.
3 The addition of CF_3 groups to the triple-hexagon junctions (THJs) is known to be extremely energetically unfavorable for hollow fullerenes (there are no structurally characterized $C_{60+x}(CF_3)_{n\leq 16}$ compounds with such motifs). In contrast, we found that the addition of CF_3 groups to THJ of the $Sc_3N@C_{80}$ cage produces stable structures starting from $Sc_3N@C_{80}(CF_3)_n$ with n = 8 (isomers with n = 6 have not yet been studied in detail). Derivatives with n = 8, 10, 12, and 14 were found to have one CF_3 group bonded to THJ (**Sc-8-1**, **Sc-8-2**, **Sc-10-1**, **Sc-12-1**, and **Sc-14-2**). Moreover, **Sc-14-1** and **Sc-16-1** have four and eight THJ-bonded CF_3 groups, respectively. This analysis demonstrates that the addition of CF_3 groups to THJs of $Sc_3N@C_{80}$ cage can be favorable even at the moderate stages of trifluoromethylation (with relatively few CF_3 groups attached to the cage).

In summary, the presence of Sc_3N cluster inside the cage brings about significant deviations to the general trends that govern trifluoromethylation of the hollow fullerenes. Most of these trends are violated in the case of $Sc_3N@C_{80}$ trifluoromethylation; this is caused by two effects: (i) the electron transfer from the cluster to the cage and (ii) mixing of the cluster and cage molecular orbitals. It is instructive to analyze the addition of CF_3 groups to the $Sc_3N@C_{80}$ cage to be more or less energetically favorable relative to CF_3 additions to hollow fullerenes. Direct experimental determination of C(CF_3)−C(cage) bond energy has not been accomplished yet (due to significant experimental difficulties); the computations of such values meet serious difficulties due to the basis set superposition error, basis set incompleteness error, and the errors of the approximate description of electron exchange and correlation by DFT. Therefore, instead of trying to calculate the absolute bond energies, we have computed two types of relative bond enthalpies using $C_{60}(CF_3)_2$ as a reference to determine the enthalpies of the following isodesmic reactions:

$$\text{fullerene}(CF_3)_{n-2} + C_{60}(CF_3)_2 \rightarrow \text{fullerene}(CF_3)_n + C_{60} \quad (1)$$

$$\text{fullerene} + n/2C_{60}(CF_3)_2 \rightarrow \text{fullerene}(CF_3)_n + n/2C_{60} \quad (2)$$

where "fullerene" can stand for any kind of fullerene. The analysis of the changes in the enthalpies of the first reaction (ΔH_1's) versus n values can reveal the optimum number of added groups (it does not mean, however, that this number of groups will be realized under the actual experimental conditions in the presence of the excess of trifluoromethylation agents). The enthalpy of the second reaction (ΔH_2) measures the average addition enthalpy of the given number of groups n, where n is an even integer. Table 2 lists ΔH_1 and ΔH_2 values normalized to the number of CF_3 groups for n up to 18 for C_{60} and C_{70}, and up to 16 for $Sc_3N@C_{80}$ computed at the PBE/TZ2P level; the lowest-energy isomers were chosen for each composition.

A further addition to fullerene$(CF_3)_n$ should be favorable if ΔH_1 for the addition of the next pair of CF_3 groups is lower than ΔH_1 for the addition of the previous pair of CF_3 groups. According to this criterion, the addition of up to six CF_3 groups

Table 2. Enthalpies (kJ/mol) of Isodesmic Reactions of Trifluoromethylated Fullerenes with $C_{60}(CF_3)_2$

	ΔH_1	ΔH_2		ΔH_1	ΔH_2		ΔH_1	ΔH_2
60-2-1	0.0	0.0	**70-2-1**	7.2	7.2	**Sc-2-1**	5.4	5.4
60-4-1	−1.3	−0.7	**70-4-1**	2.5	4.9	**Sc-4-1**	11.4	8.4
60-6-1	−3.0	−1.4	**70-6-1**	0.5	3.4	n/a		
60-8-3	1.5	−0.7	**70-8-1**	−6.6	0.9	**Sc-8-2**	15.4	11.9
60-10-6	10.3	1.5	**70-10-1**	6.5	2.0	**Sc-10-1**	13.6	12.2
60-12-1	3.9	1.9	**70-12-2**	19.8	5.0	**Sc-12-1**	19.3	13.4
60-14-1	33.4	6.4	**70-14-1**	22.8	7.5	**Sc-14-1**	28.2	15.5
60-16-3	27.4	9.0	**70-16-1**	20.6	9.2	**Sc-16-1**	28.1	17.1
60-18-C_{3v}	27.3	11.1	**70-18-1**	21.3	10.5			

is most favorable for C_{60}; the following addition that leads to **60-8-3** is slightly less favorable; starting from n = 10, further addition of pairs of CF_3 groups becomes significantly less favorable (note that the formation of the especially stable addition pattern of **60-12-1** results in the small ΔH_1 value for **60-12-1** and the large ΔH_1 value for **60-14-1**). On average, ΔH_2 changes weakly up to n = 12; then it shows a pronounced trend to grow from 1.5 for **60-10-6** up to 11.0 kJ/mol for **60-18-1**. Interestingly, the first addition step (of a pair of CF_3 groups) to C_{70} is 7.2 kJ/mol less favorable than for C_{60} (this lies in agreement with a lower reactivity of C_{70} toward trifluoromethylation that was established experimentally[42]); the further additions up to **70-8-1** are energetically favorable. Starting from **70-10-1**, each subsequent step becomes less favorable (except for n = 16); however, the ΔH_1 values for $n(CF_3)$ from 12 to 18 are very close. On the scale of the average addition enthalpy (ΔH_2), one can see a decrease of ΔH_2 values up to n = 8, followed by a gradual increase of ΔH_2 values up to 10.5 kJ/mol for n = 18. Note that for the large n values of 16 and 18, ΔH_2 values for C_{60} and C_{70} are almost identical. A noticeably different trend was found for $Sc_3N@C_{80}$. Each subsequent addition is less favorable than the previous one, starting from the addition of the first two CF_3 groups, with the only exception being **Sc-8-2** (addition to this compound is slightly more favorable). Similarly, ΔH_2 increases steadily over the whole range of n values. Importantly, the increase of ΔH_1 and ΔH_2 values with the number of added groups is much faster than for C_{60} and C_{70} (cf., for n = 16, ΔH_2 values are 21.6 kJ/mol for C_{60}, 20.6 kJ/mol for C_{70}, and 28.1 kJ/mol for $Sc_3N@C_{80}$). Therefore, the data in Table 2 show that addition of CF_3 groups to $Sc_3N@C_{80}$ is less energetically favorable than CF_3 addition to C_{60} and C_{70}. This explains the fact that in the experiments with a large excess of trifluoromethylating reagents (see above) the maximum number of added groups reached 22 for C_{60} and C_{70}, whereas for $Sc_3N@C_{80}$ the limit was found to be 20. This counterintuitive result (one might expect a larger number of added groups for a larger carbon cage) can also be explained by the nature of cluster−cage interactions in $Sc_3N@C_{80}$. Scandium atoms are bonded to fullerene via d−π interactions which are characterized by the gradual decrease of Sc−C bond orders with the distance (rather than abrupt changes of the bond strength with the distance, which is typical for localized bonds). Therefore, each scandium atom cuts an island of several carbon atoms of the cage to which it is bonded and which are, therefore, inaccessible for exohedral derivatization.

2.3.4. X-ray Structural Studies. For growing single crystals suitable for X-ray diffraction we used a technique based on the slow solvent evaporation. The crystals grown from the *p*-xylene solution of **Sc-10-1** formed a solvate $Sc_3N@(C_{80}\text{-}I_h)(CF_3)_{10}\cdot 1.5C_8H_{10}$, and the **Sc-12-1** sample dissolved in carbon disulfide formed a solvate $Sc_3N@(C_{80}\text{-}I_h)(CF_3)_{12}\cdot CS_2$. The small size (9−88 μm) of the obtained crystals required the use of synchrotron radiation to perform crystallographic studies; this allowed us to determine the structures of **Sc-10-1** and **Sc-12-1** with high precision.

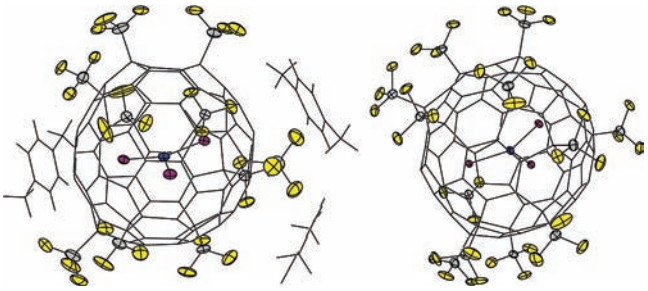

Figure 6. X-ray structures (50% thermal ellipsoids) of **Sc-10-1** (left) and **Sc-12-1**(right).

2.3.4.1. 1,3,7,17,24,28,39,47,51,62-$Sc_3N@(C_{80}\text{-}I_h)(CF_3)_{10}$. The X-ray structural data for **Sc-10-1** confirmed the addition pattern that we predicted on the basis of ^{19}F NMR/DFT analysis (see above). It consists indeed of one isolated CF_3 group and an "*S*-shaped" ribbon of six edge-sharing *p*-$C_6(CF_3)_2$ hexagons and two 1,3-$C_5(CF_3)_2$ pentagons, or a ribbon of nine CF_3 groups (Figure 6). In contrast to the published crystallographic data for the parent $Sc_3N@(C_{80}\text{-}I_h)$ and most of the studied cycloadducts (see Table SI-3 in SI for examples), the X-ray structure of **Sc-10-1** reveals that the Sc_3N cluster has only one orientation that is significantly more stable than the alternative orientations. Furthermore, as a result of the addition of 10 trifluoromethyl groups to the cage, a considerable distortion of the cluster from the idealized D_{3h} symmetry occurs. This was also observed in the crystal structures of **Sc-14-1** and **Sc-16-1** isomers.[16] Figure 7a shows that one Sc1−N−Sc3 angle in **Sc-10-1** is 119.2(2)° (still close to 120° in the underivatized $Sc_3N@(C_{80}\text{-}I_h)$), but Sc2−N−Sc3 and Sc1−N−Sc2 are 105.5(2) and 135.3(2)°, respectively. The distance between the nitrogen atom and a centroid of Sc atoms is 0.170 Å. Despite the angular distortion, the Sc_3N cluster is still planar within 0.016 Å, and Sc−N bond lengths are 2.005(4), 2.031(4), and 2.031(4) Å, which are close to Sc−N distances (1.993(1)−2.053(1) Å) in the unmodified $Sc_3N@(C_{80}\text{-}I_h)$. Each scandium atom coordinates to two C−C bonds on the cage: Sc1···C12−C13 and Sc1···C13−C31 distances are respectively 2.174(5) and 2.205(5) Å; Sc2···C22−C43 and Sc2···C42−C43 distances are respectively 2.158(5) and 2.196(5) Å; Sc3···C76−C80 and Sc2···C74−C76 distances are respectively 2.152(5) and 2.171(5) Å (Figure 7b and Figure SI-15a−c (SI)). The Sc−C distances from Sc1, Sc2, and Sc3 to the closest cage carbon atoms C13, C43, and C74 are respectively 2.275(5), 2.264(5), and 2.254(5) Å (Figure SI-15a−c, SI). The centroid of all cage carbons is shifted 0.257(5) Å from the centroid of three scandium atoms and 0.089 Å from the nitrogen atom as shown in Figure 8.

2.3.4.2. 1,3,7,17,24,28,39,47,51,54,62,70-$Sc_3N@(C_{80}\text{-}I_h)(CF_3)_{12}$. The X-ray crystallographic study confirmed our conjecture based on the NMR/DFT analysis that the addition pattern of **Sc-12-1** has a subpattern of the structure of **Sc-10-1**, and the former is obtained by the addition of two CF_3 groups to the C54 and C70 carbon atoms (Figure 6). Thus, the **Sc-12-1** addition pattern contains a ribbon made of seven edge-sharing

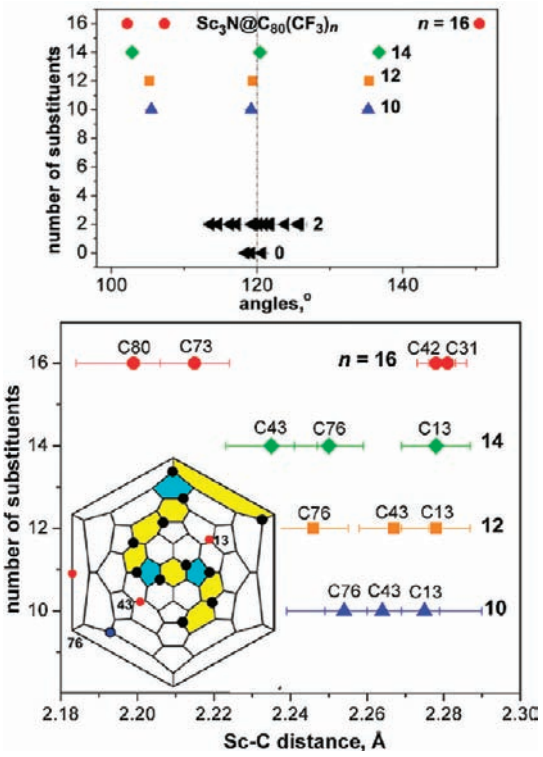

Figure 7. (a) The X-ray-determined Sc−N−Sc angles in the Sc_3N cluster for $Sc_3N@C_{80}(CF_3)_n$ with n = 10, 12, 14, and 16. Literature X-ray data for $Sc_3N@C_{80}X_2$ include the structures of monocycloadducts and bisadducts with two independent groups on the cage. (b) The X-ray determined shortest distances from Sc atom to the closest cage carbon atom in $Sc_3N@C_{80}(CF_3)_n$ with n = 10, 12, 14 and 16: the distances from Sc1 to C12−C13 and C13−C31 bonds are 2.174(5)−2.183(3) Å and 2.194(3)− 2.205(5) Å; from Sc2 to C22−C43 and C42−C43 bonds are 2.147(3)−2.158(5) and 2.189(5)−2.203(3) Å; from Sc3 to C76−C80 and C74−C76 bonds are 2.147(3)−2.152(5) Å and 2.170(3)−2.171-(5) Å, respectively. The minor change in the position of Sc2 atom, which is closer to C22−C43 (2.148(4) Å) bond and equidistant to two C42−C43 and C43−C44 bonds (2.189(4) Å), was observed in the structure of **Sc-14-1**. In contrast, Sc2 atom in the **Sc-10-1** and **Sc-12-1** structures coordinates only to two bonds, C22−C43 and C42−C43, respectively. The numbers of the closest cage carbon atoms are labeled on the Schlegel diagram of **Sc-12-1** as an example.

p-$C_6(CF_3)_2$ hexagons and three 1,3-$C_5(CF_3)_2$ pentagons, and one isolated CF_3 group attached to THJ. As in the case of the **Sc-10-1**, only one Sc_3N orientation is observed, and the trimetallic nitride cluster is planar within 0.008 Å. As one might expect, the geometrical parameters of Sc_3N such as Sc−N−Sc angles and Sc−N bond lengths are very similar to those in the **Sc-10-1** structure. One of the Sc1−N−Sc3 angles is close to 120° (119.4(2)°), and Sc2−N−Sc3 and Sc1−N−Sc2 are 105.2(2) and 135.4(2)°, respectively (Figure 7a). The Sc−N bond lengths are 2.002(4), 2.038(4), and 2.045(4) Å. In addition, Sc atoms coordinate to the exact same C−C bonds as observed in the **Sc-10-1** crystal structure. The distances from Sc1 to the C12−C13 and C13−C31 bonds are respectively 2.183(3) and 2.194(3) Å; from Sc2 to two close C22−C43 and C42−C43 bonds are respectively 2.147(3) and 2.203(3) Å; from Sc3 to two close C76−C80 and C74−C76 bonds are 2.147(3) and 2.170(3) Å, respectively. The Sc−C distances from Sc1, Sc2, and Sc3 to the closest cage carbon atoms C13, C43, and C76 are 2.278(3), 2.267(3), and 2.246(3) Å, respectively (see Figure 7b and Figure SI-16a−c in the SI). The shift of the cage carbon atom centroid is 0.256(3) Å relative to the centroid of Sc atoms and 0.089 Å to the nitrogen atom (Figure 8). The Sc−N distance between the scandium atom centroid and the nitrogen atom is 0.168(3) Å.

*2.3.5. Geometry and Position of the Sc_3N Cluster in the **Sc-10-1**, **Sc-12-1**, **Sc-14-1**, and **Sc-16-1** Structures.* The mutual effects of the cluster and CF_3 groups attached to the cage were first discussed in our X-ray crystallographic studies of **Sc-14-1** and **Sc-16-1**.[16] The new X-ray crystal structures of **Sc-10-1** and **Sc-12-1** have addition patterns reminiscent to that of **Sc-14-1** (an "*S*-shaped ribbon"). The addition pattern of **Sc-16-1** is, however, very different. It contains CF_3 groups arranged in the double loop of the edge-sharing p-$C_6(CF_3)_2$ hexagons.[16]

The structural parameters of all four compounds were determined with high precision and accuracy, which provides an opportunity (still rare in the MNF research) to study correlations between the geometrical parameters, number of substituents, and their addition patterns and to carry in-depth analysis of the dynamics of Sc_3N cluster inside the fullerene cage.

The correlation between Sc−N−Sc angles and the number of the attached substituents (X) in the $Sc_3N@(C_{80}\text{-}I_h)(X)_n$ compounds with the known crystal structures is plotted in Figure 7a. This analysis includes four known structures of $Sc_3N@(C_{80}\text{-}I_h)$-$(CF_3)_n$, parent $Sc_3N(C_{80}\text{-}I_h)$,[58] three structures of monoadducts $Sc_3N@(C_{80}\text{-}I_h)(X)$ where X = $C(C_6H_5)_3NC_2H_4$,[55] $C(C_6H_5)(CH_2CH_2CH_2COOCH_3)$,[59] $(C_{10}H_{12}O_2)$,[60] and two structures of bisadducts, $Sc_3N@(C_{80}\text{-}I_h)(CH_2C_6H_5)_2$,[37] and $Sc_3N@C_{80}((C_6H_2(CH_3)_2Si)_2CH_2$.[50]

This plot reveals that in the $Sc_3N@(C_{80}\text{-}I_h)$ derivatives, the Sc_3N cluster deviates from the 3-fold symmetry, and as the number of the attached groups increases, it experiences larger and larger angle distortions. The Sc−N−Sc angles in the cluster of the naked $Sc_3N@C_{80}$ cage are very close to 120° (118.5(1), 119.6(1), and 120.7(1)).[58] The presence of two substituents (or a cycloadduct) on the $Sc_3N@C_{80}$ cage leads to small deviations in the Sc−N−Sc angles from 120°, and the observed range for the $Sc_3N@(C_{80}\text{-}I_h)X_2$ is 113.6(3)−125.9(3)°. For the $Sc_3N@$-$(C_{80}\text{-}I_h)(CF_3)_n$ compounds with n = 10 and 12, drastic changes in the cluster geometry are observed: two of the three Sc−N−Sc angles deviate from 120° to become 105° and 135°. The maximum angle distortion occurs in the **Sc-16-1** structure, in which all three angles deviate from 120°: 102.2(2), 107.1(1), and 150.5(1)°. Remarkably, such strong in-plane cluster distortions give no deviations from planarity of the cluster for any of the structures.

Three Sc−N bonds have different lengths in the unmodified $Sc_3N@(C_{80}\text{-}I_h)$ as found from its crystal structure (Figure SI-17, SI). After addition of 10 CF_3 groups to the cage in **Sc-10-1**, two Sc−N bonds have identical lengths (2.031(4) Å). The same tendency is observed in the **Sc-12-1** and **Sc-14-1** structures: two Sc−N bonds have very close bond length values. In **Sc-16-1**, Sc−N distances are in the narrower range (2.0027(13)−2.013(2) Å) compared to 1.997(3)−2.051(3) Å observed for **Sc-10-1**, **Sc-12-1**, and **Sc-14-1** structures. Overall, these variations are not considerable, and we can conclude that a deviation of trimetallic nitride cluster from the idealized D_{3h} symmetry occurs mainly due to distortion of Sc−N−Sc angles.

The same cluster orientation inside the fullerene cage was observed in **Sc-10-1**, **Sc-12-1**, and **Sc-14-1** crystal structures. Figure 7b shows that one of the Sc atoms in these three structures is always close to C76, C43, and C13 cage carbons. The distances

dx.doi.org/10.1021/ja109462j |*J. Am. Chem. Soc.* 2011, 133, 2672–2690

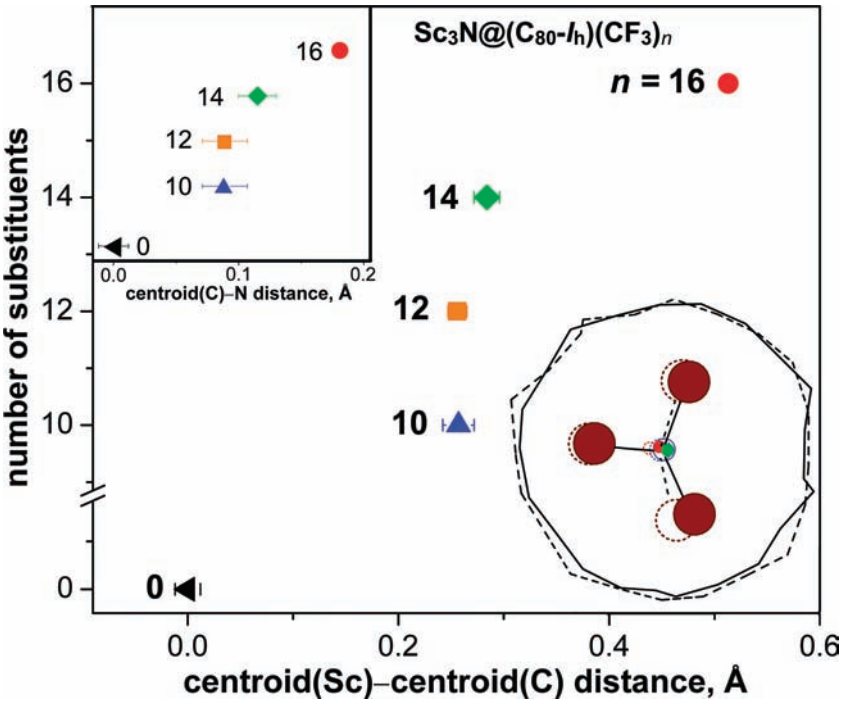

Figure 8. X-ray-determined distances from cage carbon atoms to the centroid of Sc atoms in the Sc_3N cluster on the number of CF_3 groups. The inset (left) shows the dependence of the distance from the nitrogen atom to the scandium atom centroid on the number of CF_3 groups. The inset (right) shows the shift of the Sc_3N cluster in **Sc-16-1** (dashed line) compared to the one in **Sc-10-1** (solid line). Centroids of **Sc-16-1** and **Sc-10-1** carbon cages are superimposed (green dot).

from each Sc atom to the closest C−C bond are also similar for three structures, as shown in Figure 7b. In **Sc-16-1**, the Sc_3N cluster changes its location, and three scandium atoms become close to the C80, C73, C42, and C31 (C13) carbon atoms.

In Figure 8, the dependence of the cluster position on the number of trifluoromethyl groups is shown. The centroid of the cage carbons is considered as a center of the fullerene cage, and both the nitrogen atom and the centroid of scandium atoms represent the center of Sc_3N cluster. In the unmodified $Sc_3N@(C_{80}\text{-}I_h)$ cage centroids of Sc and C atoms, and N atom are on the same site. The addition of 10 CF_3 groups leads to the shift of Sc_3N cluster from the center of the cage as it is demonstrated by the centroid(C)−centroid(Sc) and centroid(C)−N distances: 0.257(5) Å and 0.089(6) Å, respectively. Further attachment of two or even four CF_3 groups does not significantly affect the position of the cluster, and the centroid(C)−centrod(Sc) and centroid(C)−N distances are 0.256(3)−284(4) and 0.089(6)−0.115(5) Å, respectively. In contrast, in the **Sc-16-2** structure the centroid of cage carbons is shifted 0.513(3) Å from the centroid of Sc atoms and 0.181(2) Å from N atom. To estimate the effect of cage distortion due to the formation of sp^3 carbon atoms, a new artificial $C_{80}(I_h)$ cage was constructed. Carbon atoms connected to CF_3 groups were replaced by the centroids of the nearest three C atoms. The coordinates of these centroids were adjusted to achieve curvature of the $C_{80}(I_h)$ cage by moving them 0.220(5) Å in the direction from the center of the fullerene cage. It was found that the distance from the centroid(C*) of the "idealized" $C_{80}(I_h)$ cage to the centroid(C*) of the actual distorted cage is no longer than 0.026(2) Å (Table SI-2, SI). So, the shift of the centroid(C)−centroid(Sc)/centroid(C*)−centroid(Sc) (0.257(4)/0.243(4) Å) and centroid(C)−N/centroid(C*)−N (0.092(6)/0.077 Å) distances in **Sc-16-1** compared to **Sc-12-1** (**Sc-10-1**) structure is almost the same as the one observed between **Sc-12-1** (or **Sc-10-1**) and naked $Sc_3N@(C_{80}\text{-}I_h)$. Thus, a drastic change of the addition pattern in **Sc-12-1** (or **Sc-10-1** and **Sc-14-1**) structure as compared to the one in the **Sc-16-1** structure has as strong effect on the cluster position as the change observed when the unmodified $Sc_3N@(C_{80}\text{-}I_h)$ is compared with **Sc-12-1** structure. Therefore, it is the addition pattern, and not the number of the groups, that plays more important role in the observed cluster location and geometry.

2.3.5.1. Packing in the $Sc_3N@(C_{80}\text{-}I_h)(CF_3)_n$ Crystals. The crystal lattices of the **Sc-10-1**, **Sc-12-1**, and **Sc-14-1** structures contain *p*-xylene, carbon disulfide, and *p*-xylene molecules, respectively, whereas no solvent was incorporated into the **Sc-16-1** lattice (Figure 9 and Figure SI-17a,b in the SI). Each **Sc-10-1** molecule is surrounded by six molecules in one layer and by three others in the top and bottom layers, which leads to the formation of the distorted hexagonal cubic packing (*hcp*). In the **Sc-12-1** structure, one fullerene molecule is also surrounded by six others, but four molecules are located in the top layer, and two fullerene molecules are in the bottom layer (Figure SI-17a, SI). The distorted cubic close packing was observed in the **Sc-14-1** and **Sc-16-1** crystal structures (Figures 9 and SI-17b [SI]). The closest intermolecular F···F distances between trifluoromethylated $Sc_3N@(C_{80}\text{-}I_h)$ molecules in **Sc-10-1**, **Sc-12-1**, **Sc-14-1**, and **Sc-16-1** are 2.897(4) (F072···F623), 2.720(3) (F172···F622), 2.695(5) (F511···F623), and 2.550(2) Å (F162···F463), respectively.

Figure 9 demonstrates that *p*-xylene molecules form layers in the **Sc-10-1**·$1.5C_8H_{10}$ and **Sc-14-1**·$0.5C_8H_{10}$ crystal structures. Previously, formation of the channels made of *p*-xylene molecules was also observed in the $C_{74}(CF_3)_{12}\cdot 3C_8H_{10}$ structure.[44] Thus, in the case of highly substituted trifluoromethylated endo-

dx.doi.org/10.1021/ja109462j |*J. Am. Chem. Soc.* 2011, 133, 2672–2690

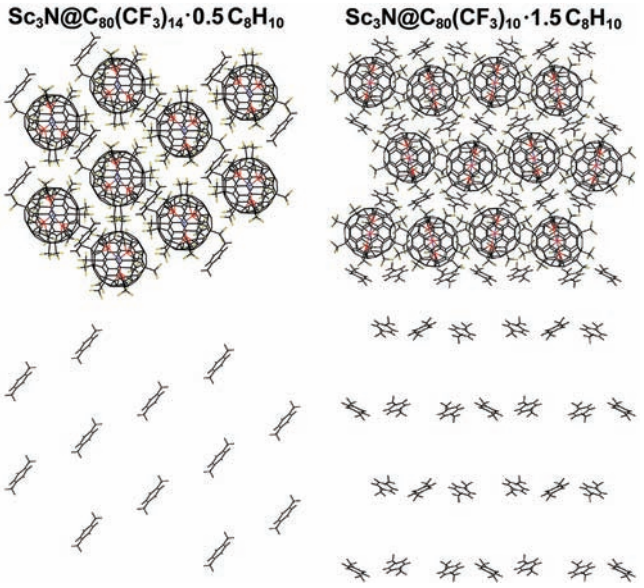

Figure 9. Packing of **Sc-14-1** (left) and **Sc-10-1** (right) molecules in the crystal lattice. The *p*-xylene molecules form layers which may prevent the rotational disorder of fullerene cage.

metallofullerenes, aromatic hydrocarbons may play a role analogous to that of the porphyrin molecules which are used for cocrystallization with naked fullerenes (Figure SI-18, SI).[61] The arrangements of three solvent molecules (*p*-xylene) and **Sc-10-1** in the crystal structure of $Sc_3N@(C_{80}\text{-}I_h)(CF_3)_{10}\cdot 1.5C_8H_{10}$ form effective packing in the crystal lattice and may explain the absence of the positional cage disorder. In contrast, cage disorder has been commonly observed in the structures of the $Sc_3N@(C_{80}\text{-}I_h)$ cycloadducts (Table SI-3, SI).

2.3.6. Charge and Energy of the Sc_3N Cluster. It is commonly accepted that the electronic structure of $Sc_3N@C_{80}$ can be described as a result of a formal 6-fold electron transfer from the cluster to the carbon cage.[62,63] A significant degree of covalency results in much smaller actual charges (atomic charges are not uniquely defined and are different from method to method,[64−66] but no matter what method is used to determine the charges in $Sc_3N@C_{80}$, their values are, at maximum, half of those expected for the complete ionic scheme). It is instructive to analyze how the attachment of different numbers of electron-withdrawing CF_3 groups affects the charge distribution in $Sc_3N@C_{80}$. For an analysis of atomic charges, we have chosen Bader's QTAIM approach as physically sound and weakly dependent on the method of theory/basis set used to calculate the wave function of the molecule (see ref 65 for a detailed analysis of bonding in EMFs using QTAIM). Table 3 lists net Bader charges of CF_3 groups, Sc_3N cluster, and a carbon cage. An electron-withdrawing effect of CF_3 groups is manifested in their negative charges, ∼−0.12 (compare to the charge of −0.11 in $C_{60}(CF_3)_{12}$ determined by the topological analysis of the experimentally determined electron density).[67] This value is, however, not constant and tends to decrease with the increase of *n*, from −0.137 in **Sc-2-1** to −0.109 in **Sc-16-1** (note that the range of individual values in one molecule can be rather large, e.g. from −0.095 to −0.139 in **Sc-14-1**). Even though the cumulative effect of CF_3 groups can be rather large (up to 1.744 electrons in **Sc-16-1**), it has only marginal effect on the cluster charge. Moreover, except for **Sc-16-1**, the charge of the cluster is even

Table 3. Bader Charges (*q*) and Relative Atomic Energies (Δ*E*, kJ/mol) and DFT-Computed HOMO−LUMO Gaps in $Sc_3N@C_{80}(CF_3)_n$ Derivatives[a]

	q				Δ*E*			gap
	CF_3	Sc_3N	C_{80}	$\pi\text{-}C_{80-2n}$[b]	N	Sc	Sc_3N	PBE
$Sc_3N@C_{80}$		3.496	−3.496	−3.496	0	0	0	1.463
Sc-2-1	−0.137	3.444	−3.170	−3.312	19	75	243	1.149
Sc-4-1	−0.134	3.398	−2.862	−3.146	−58	94	224	1.103
Sc-8-1	−0.132	3.355	−2.301	−2.878	−40	187	521	1.127
Sc-8-2	−0.134	3.357	−2.286	−2.892	−51	184	500	1.152
Sc-10-1	−0.129	3.317	−2.028	−2.767	−2	236	707	1.079
Sc-12-1	−0.125	3.287	-1.791	−2.668	−8	252	747	1.238
Sc-12-2	−0.120	3.305	−1.859	−2.767	−3	255	762	1.239
Sc-14-1	−0.124	3.258	-1.524	−2.557	−31	245	706	1.415
Sc-14-2	−0.118	3.280	−1.632	−2.672	−7	272	809	1.358
Sc-16-1	−0.109	3.379	−1.634	−2.805	−73	288	790	1.620

[a] Bader analysis is performed for B3LYP/6-311G*//PBE/TZ2P electronic densities, HOMO−LUMO gaps are computed at the PBE/TZ2P level. [b] $\pi\text{-}C_{80-2n}$ denotes the π part of the carbon cage.

decreasing with *n* (from 3.496 in $Sc_3N@C_{80}$ to 3.258 in **Sc-14-1**). That is, instead of the intuitively expected further polarization of Sc-cage bonds by the electron withdrawal from the carbon cage, the opposite effect is found: the charge of the carbon cage, which is decreasing from −3.496 in $Sc_3N@C_{80}$ to −1.524 in **Sc-14-1**, is not compensated by the additional electron transfer from the cluster. Certainly, a substantial part of the charge of the carbon cage is due to the positive charges of CF_3-bearing sp^3-hybridized carbon atoms (∼+0.07 each), but even if the charges of these atoms are subtracted, the resulting charges of the carbon π systems in $Sc_3N@C_{80}(CF_3)_n$ molecules (column 5 in Table 3) still exhibit pronounced tendency to decrease with the increase of the number of CF_3 groups.

In addition to the determination of charges, partitioning of the electron density into atomic basins in QTAIM allows determination of the energies of the atoms, which are additive values, and they add up to the total energy of the molecule.[68,69] Therefore, it is possible to compute the energies of the groups of atoms and to follow the changes in the energies in a series of similar compounds (note that the absolute values of the energies are of little interest). The changes of the Sc_3N cluster geometry with the number of CF_3 groups motivated us to study the energy of the cluster. Table 3 lists relative energies of N and Sc atoms and the Sc_3N cluster in the selected $Sc_3N@C_{80}(CF_3)_n$ derivatives with respect to the values in $Sc_3N@C_{80}$. Except for **Sc-2-1**, the energy of nitrogen atoms is somewhat lower than in $Sc_3N@C_{80}$; however, the Sc atoms exhibit strong increase the number of CF_3 groups (up to 288 kJ/mol in **Sc-16-1**). Accordingly, the energy of the whole Sc_3N cluster is also increasing dramatically. Thus, distortion of the cluster results in a strong increase of its energy. It is not possible at this time to deduce which part of this large energy change is due to the cluster distortion and which is caused by other reasons (change of the charge, etc.), but in any case, it is clear that an increase in the number of CF_3 groups destabilizes the cluster.

2.4. Electronic Properties. Addition of CF_3 groups to the fullerene cage dramatically changes the electronic properties of fullerenes and can result in an either stronger or weaker electron acceptor, depending on the addition pattern.[25] Earlier we have

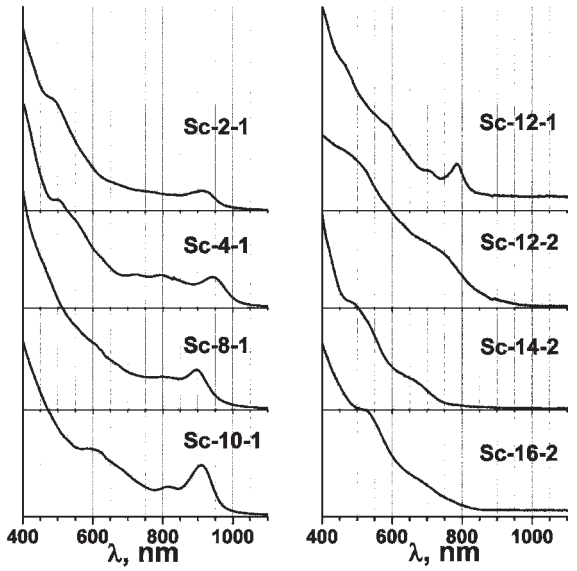

Figure 10. Vis−NIR absorption spectra (toluene) of the select $Sc_3N@C_{80}(CF_3)_n$ derivatives.

shown that addition of two CF_3 groups to $Sc_3N@C_{80}$ reduces its optical gap (defined here as the energy of the lowest energy transition in the vis−NIR spectrum) and redox potentials of $Sc_3N@C_{80}(CF_3)_2$ are shifted by +0.10 and −0.15 V for reduction and oxidation, respectively.[17,18] Figure 10 shows the vis−NIR absorption spectra of a series of $Sc_3N@C_{80}(CF_3)_n$ derivatives. Optical gap of **Sc-4-1**, 1.31 eV is even smaller than that of **Sc-2-1** (1.35 eV), but for the compounds with a larger number of CF_3 groups the gap is increasing from 1.38 eV in **Sc-8-1** to 1.84 eV in **Sc-14-1**. The DFT-computed HOMO−LUMO gaps of the derivatives show the same trend as the experimental values (Table 4): first, a decrease of the gap after addition of a few CF_3 groups to $Sc_3N@C_{80}$ and then an increase at later stages of addition. Importantly, the variation of the gaps in the series of these derivatives can be roughly correlated with their relative yields observed experimentally. It can be anticipated that the smaller gap points to the higher reactivity of the derivative. Hence, one can expect that derivatives with smaller gaps are not accumulated in the reaction mixture since they react faster with formation of the products with higher numbers of groups that have larger gaps. This reasoning can explain the small yield of **Sc-4** isomers; probably, extremely low yields of **Sc-6** isomers are also caused by this. The increase of the gap with the increase of the number of CF_3 groups also agrees with the increase of the yields of the derivatives with larger numbers of CF_3 groups.

Cyclic voltammetry curves for the selected $Sc_3N@C_{80}(CF_3)_n$ derivatives are shown in Figure 11. In contrast to the parent $Sc_3N@C_{80}$, that exhibits irreversible reductions at moderate electrochemical scan rates,[70,71] all studied $Sc_3N@C_{80}(CF_3)_n$ give a reversible first reduction step; for **Sc-2-1**, **Sc-10-1**, and **Sc-12-1**, the second and third reduction steps are also reversible at a scan rate of 20 mV s^{-1}, whereas a more complex electrochemical pattern is observed at the second step for **Sc-4-1**. All studied derivatives are stronger electron acceptors than $Sc_3N@C_{80}$: the $E_{1/2}$ potential for 0/− is positively shifted with respect to the value for $Sc_3N@C_{80}$ by +0.10 V in **Sc-2-1**, +0.20 V in **Sc-4-1**, +0.42 V in **Sc-10-1**, and +0.31 V in **Sc-12-1** (Table 4). Fully electrochemically reversible oxidation is observed only for **Sc-2-1**, whose potential, as noted above, is shifted cathodically by

Table 4. Redox Potentials of $Sc_3N@C_{80}(CF_3)_n$ Derivatives[a]

	2+/1+	1+/0	0/1−	1−/2−	2−/3−	gap (EC)	gap (Opt)
$Sc_3N@C_{80}$	2.35	1.85	0.00	−0.36	−1.11	1.85	1.69
Sc-2-1	1.92	1.69	0.10	−0.39	−0.88	1.59	1.35
Sc-4-1		1.81[b]	0.20	−0.29[b]	−0.77	1.61	1.31
Sc-10-1		2.12[b]	0.42	−0.06	−0.85	1.70	1.36
Sc-12-1		2.21[b]	0.31	−0.12	−0.72	1.90	1.58

[a] Values are given vs reversible potential of $Sc_3N@C_{80}^{0/-}$ redox pair measured at high scan rates; $E_{1/2}$ of $Sc_3N@C_{80}^{0/-}$ pair vs $Fe(Cp)_2^{+/0}$ is 1.26 V.[71] [b] Poorly reversible steps.

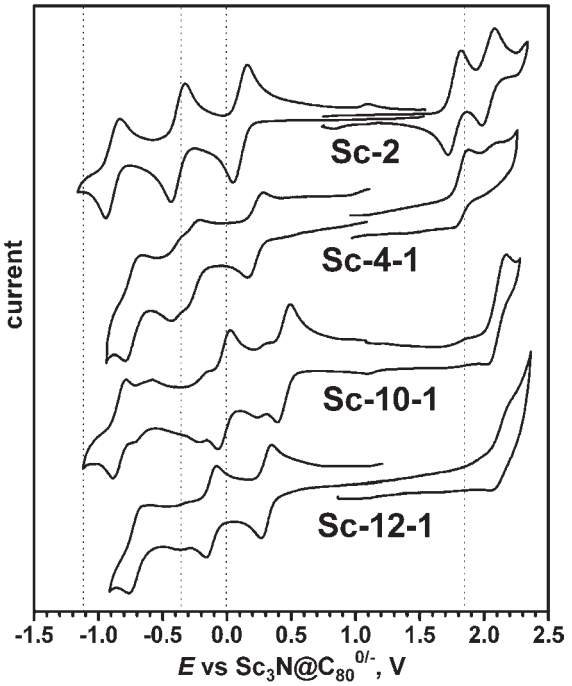

Figure 11. Cyclic voltammograms of selected $Sc_3N@C_{80}(CF_3)_n$ derivatives (room temperature, 0.1 M $TBABF_4$ in *o*-DCB, scan rate 20 mV·s^{-1}). Dotted vertical bars denote redox potentials of $Sc_3N@C_{80}$ (for cathodic part, $E_{1/2}$ values measured at high scan rates in ref 70 are used).

0.15 V. For the other derivatives, an increase of the number of the CF_3 groups results in a shift of the $E_{1/2}$ potential for +/0 with respect to the $Sc_3N@C_{80}$ value by −0.05 V in **Sc-4-1**, +0.27 V in **Sc-10-1**, and +0.36 V in **Sc-12-1**. As the oxidation potential is shifting toward the edge of the potential window of the solvent, the process becomes less and less reversible due to the reaction of the solvent. Electrochemical gaps (computed as the difference of the first reduction and first oxidation potentials) of derivatives qualitatively agree with the optical gaps, showing a tendency to increase with $n(CF_3)$ values as well.

It has been shown recently that MNF derivatives may outperform C_{60} derivatives as an electron-accepting block in organic photovoltaic devices.[72−74] Our work reveals that chemical derivatization of $Sc_3N@C_{80}$ with CF_3 groups yields a new family of acceptor compounds, in which their electron accepting ability can be fine-tuned with respect to $Sc_3N@C_{80}$ in the unprecedented range of redox potentials. Spatial localization of LUMO can be an important factor determining the mechanism and rates of charge transfer processes. It has been shown that in

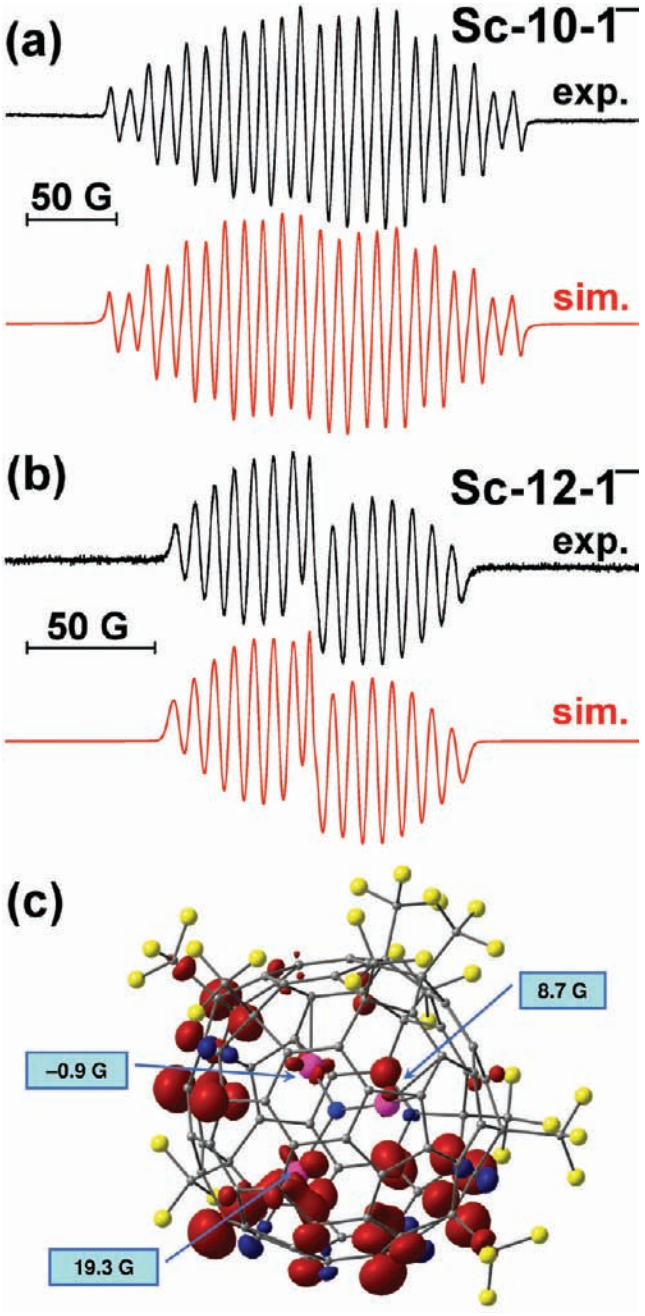

Figure 12. (a,b) Experimental (black curves) and simulated (red curves) ESR spectra of **Sc-10-1**$^-$ and **Sc-12-1**$^-$ radical anions generated by reaction with ~1 equiv of cobaltocene $Co(Cp)_2$. In simulations, the presence of single-line radical impurities was assumed (~20% in **Sc-10-1** and ~1.5% in **Sc-12-1**; the presence of ~20% impurity in **Sc-10-1** can be also seen in its cyclic voltamogramm); (c) spin density distribution and ^{45}Sc hyperfine coupling constants in **Sc-10-1**$^-$ computed at the B3LYP/6-311G*//PBE/TZ2P level with Neese's CP3P basis set[77] for Sc atoms.

$Sc_3N@C_{80}$ LUMO is largely localized on the endohedral cluster[63] (however, an extent of localization depends on the cluster orientation inside the cage;[66] for the C_3-conformer, the ground-state structure of neutral $Sc_3N@C_{80}$, ~40% of LUMO is localized on the cluster, while for the C_{3v} isomer, the lowest-state energy conformer of the monoanion $Sc_3N@C_{80}^-$, ~64% of LUMO is on the cluster; LUMO energy also significantly changes with the cluster orientation[66]).

Experimentally spatial localization of LUMO can be assessed by means of ESR spectroscopy of the radical anions. Spin density distribution in an anion resembles LUMO density, and, hence, large spin populations at Sc atoms point to the LUMO localized on the cluster. Although there is no exact correlation between spin population and ESR hyperfine coupling constant, large spin populations of Sc atoms are usually correlated with large $a(^{45}Sc)$ values. For instance, in agreement with localization of LUMO in $Sc_3N@C_{80}$ on the cluster, $Sc_3N@C_{80}^-$ exhibits large hfcc value of 55−56 G,[17,71] whereas in $Sc_3N@C_{68}^-$ with cage-localized LUMO hfcc is only 1.8 G.[76] Recently, we have reported an ESR spectrum of **Sc-2-1**$^-$ with intermediate $a(^{45}Sc)$ values, 2 × 9.3 and 10.7 G.[17] The DFT calculations have shown that the spin density in the monoanion is distributed between the cluster and the cage almost equally. In the spectrum of the trianion **Sc-2-1**$^{3-}$ one $a(^{45}Sc)$ value, 49.2 G, is close to that of $Sc_3N@C_{80}^-$, while two others are again considerably smaller, 2 × 9.3 G. Spin density in the trianion is to a large extent localized on one Sc atom, but cage contributions are also noticeable. Thus, addition of two CF_3 groups to the cage pushes cage orbitals down in energy so that they are mixed with the cluster orbital, reducing the spin population of the cluster in the monoanion. To follow this tendency in derivatives with large number of CF_3 groups, we have generated anion-radicals of **Sc-10-1** and **Sc-12-1** by reaction with $Co(Cp)_2$ in oDCB and measured their ESR spectra (Figure 12).

Both anions have shown a well-defined hyperfine structure due to ^{45}Sc atoms, and in both cases the spectral patterns clearly point to the fixed position of the cluster (i.e., each Sc atom has specific hfcc value), in contrast to the free rotation of the cluster in $Sc_3N@C_{80}^-$ and restricted rotation in **Sc-2-1**$^-$. The spectrum of **Sc-10-1**$^-$ can be best modeled by hfcc values 0.6, 11.1, and 21.5 G and a line width of 1.9 G, whereas the spectrum of **Sc-12-1**$^-$ is matched by hfc values 0.6, 7.4, and 8.1 G and a line width of 2.2 G. The *g*-factor values, 2.0009 for **Sc-10-1**$^-$ and 2.0012 for **Sc-12-1**$^-$, are closer to the free-electron value, $g = 2.0023$, than those of **Sc-2-1**$^-$ ($g = 1.9958$) and $Sc_3N@C_{80}^-$ ($g = 1.9992$) measured under the same conditions as in ref 17. It points to the smaller degree of the spin localization on the metal atoms in **Sc-10-1**$^-$ and **Sc-12-1**$^-$.

Figure 12 shows spatial spin density distribution in **Sc-10-1** computed using the DFT method at the B3LYP/(6-311G*, CP3P) level. It shows only a moderate localization of the density on the metal atoms, in agreement with the experimental data; similar spin density distribution is found in **Sc-12-1**$^-$ (not shown). The DFT-computed net spin populations of the Sc_3N cluster in **Sc-10-1**$^-$ and **Sc-12-1**$^-$ are thus 13% and 11%, considerably smaller than 42% in **Sc-2-1**$^-$ and 64% in $Sc_3N@C_{80}^-$. The DFT-computed $a(^{45}Sc)$ constants in **Sc-10-1**$^-$, −0.9, 8.7, and 19.3 G, show a perfect agreement with the experimental values confirming reliability of the DFT-computed spin density distribution.

In summary, ESR spectral parameters and DFT computations show that **Sc-10-1** and **Sc-12-1** exhibit a mixing of the cluster and cage orbitals and a reduced cluster contribution to LUMO in comparison to $Sc_3N@C_{80}$ and **Sc-2-1**. Thus, the increase in the number of CF_3 groups further stabilizes cage orbitals and results in stronger mixing of the originally cluster-based LUMO between many orbitals of the mixed nature in the $Sc_3N@C_{80}(CF_3)_n$ derivatives.

3. SUMMARY AND CONCLUSIONS

This work represents the first detailed study of the products of multiple radical additions to $Sc_3N@(C_{80}\text{-}I_h)$. We have isolated

many pure $Sc_3N@(C_{80}\text{-}I_h)(CF_3)_n$ isomers with n values ranging from 2 to 16, which allowed us to study effects of the substitution degree on various physical, chemical, and electronic properties of these derivatives.

An experimental and computational study of the CF_3-addition motifs to $Sc_3N@C_{80}$ revealed a special role played by the endohedral cluster in determining chemical properties of $Sc_3N@C_{80}$. In earlier studies of CF_3 addition to higher fullerenes, we formulated general rules that govern such reactions, the most important being avoidance of the CF_3 addition to triple-hexagon junctions and preferential addition of only one CF_3 group in one pentagon (at least, at the earlier stages of addition). The present study shows that virtually all rules are violated in perfluoalkylation of $Sc_3N@C_{80}$. The lowest energy isomers of $Sc_3N@C_{80}(CF_3)_8$ have several $C_5(CF_3)_2$ units in their structure, and this feature is preserved (or increased in numbers) in the derivatives with a larger number of CF_3 groups. Starting from $Sc_3N@C_{80}(CF_3)_8$ isomers, at least one THJ-added CF_3 group is present in the most stable isomer, and the number of the THJ-added CF_3 groups reaches half of all CF_3 groups in the structurally characterized $Sc_3N@C_{80}(CF_3)_{16}$ (**Sc-16-1**). Thus, addition of CF_3 groups is to a large extent governed by the endohedral cluster. On the other hand, we show that this is a two-way influence since the CF_3 addition motif has a strong influence on the geometry of the Sc_3N cluster; the largest observed distortions of the geometry of the cluster are reported in this study.

C_{60} derivatives are by far the most widely used electron-accepting building blocks in organic photovoltaics. Recent studies have shown that functionalized $Sc_3N@C_{80}$ provides longer lifetimes of the charge-separation states compared to C_{60} derivatives in the analogous donor−acceptor dyads. Thus, $Sc_3N@C_{80}$ can be viewed as a candidate for replacement of C_{60} for creation of even more efficient dyads. In this work we show that perfluoroalkylation can be used as a tool to fine-tune electronic properties of the $Sc_3N@C_{80}$ core. For example, the first reduction potential of **Sc-10-1** is 0.42 V positively shifted compared to $Sc_3N@C_{80}$, and derivatives with different number of CF_3 groups (and different addition patterns) can be chosen if specific redox potential values $E_{1/2}$ are desired. The ESR spectroscopic study of the radical-anions has shown that perfluoroalkylation significantly affects the way how LUMO is spatially localized. While in the bare $Sc_3N@C_{80}$ LUMO is mostly based on the cluster, the increase of the number of CF_3 groups results in the stabilization of the cage MOs and their mixing with the cluster-based orbital. As a result of these changes in the electronic structure in combination with the observed reduced aggregation and thereby enhanced molecular solubility, chemical reactivity of perfluoroalkylated $Sc_3N@C_{80}$ changes drastically too. For example, a number of halogenation reactions that are commonly used for hollow fullerenes did not yield any halogenated products. At the same time, a series of preliminary studies reported here demonstrate that many reactions occur more readily with $Sc_3N@C_{80}(CF_3)_n$ than with underivatized $Sc_3N@C_{80}$. For example, a remarkably facile and selective Bingel−Hirsch reaction under standard conditions was observed; a photochemical benzylation resulted in multiple additions of benzyl radicals. Enhanced chemical reactivity of perfluoroalkylated $Sc_3N@C_{80}$ discovered in this study may become adopted as an important route for future designs of various MNF-based materials for practical applications, including but not limited to the water-soluble compounds for biomedical research, highly soluble and stable materials with the tunable LUMOs for photovoltaics and other emerging technologies.

■ ASSOCIATED CONTENT

Supporting Information. Experimental procedures, additional tables, figures, crystallographic files, and spectroscopic data. This material is available free of charge via the Internet at http://pubs.acs.org.

■ AUTHOR INFORMATION

Corresponding Author

janice.phillips@usm.edu; steven.stevenson@usm.edu; l.dunsch@ifw-dresden.de; a.popov@ifw-dresden.de; steven.strauss@colostate.edu; olga.boltalina@colostate.edu

■ ACKNOWLEDGMENT

We thank the Alexander von Humboldt Foundation (A.A.P., O.V.B.), the U.S. NSF (CHE-0707223, CHE-1012468, CHE-0822838, CHE-0547988, CHE-0847481), and the Colorado State University Research Foundation. ChemMatCARS Sector 15 is principally supported by the National Science Foundation/Department of Energy under Grant Number NSF/CHE-0822838. Use of the Advanced Photon Source was supported by the U.S. Department of Energy, Office of Science, Office of Basic Energy Sciences, under Contract No. DE-AC02-06CH11357. We acknowledge Dr. Z. Mazej for making $KMnF_4$ sample.

■ REFERENCES

(1) Stevenson, S.; Rice, G.; Glass, T.; Harich, K.; Cromer, F.; Jordan, M. R.; Craft, J.; Hadju, E.; Bible, R.; Olmstead, M. M.; Maitra, K.; Fisher, A. J.; Balch, A. L.; Dorn, H. C. *Nature* **1999**, *401*, 55–57.

(2) Stevenson, S.; Mackey, M. A.; Coumbe, C.; Phillips, J. P.; Elliott, B.; Echegoyen, L. *J. Am. Chem. Soc.* **2007**, *129*, 6072–6073.

(3) Stevenson, S.; Harich, K.; Yu, H.; Stephen, R. R.; Heaps, D.; Coumbe, C.; Phillips, J. P. *J. Am. Chem. Soc.* **2006**, *128*, 8829–8835.

(4) Stevenson, S.; Thompson, M. A.; Coumbe, H. L.; Mackey, M. A.; Coumbe, C. E.; Phillips, J. P. *J. Am. Chem. Soc.* **2007**, *129*, 16257–16262.

(5) Stevenson, S.; Mackey, M. A.; Thompson, M. C.; Coumbe, H. L.; Madasu, P. K.; Coumbe, C.; Phillips, J. P. *Chem. Commun.* **2007**, 4263–4265.

(6) Ge, Z. X.; Duchamp, J. C.; Cai, T.; Gibson, H. W.; Dorn, H. C. *J. Am. Chem. Soc.* **2005**, *127*, 16292–16298.

(7) Dunsch, L.; Yang, S. *Small* **2007**, *3*, 1298–1320.

(8) Chaur, M. N.; Melin, F.; Ortiz, A. L.; Echegoyen, L. *Angew. Chem., Int. Ed.* **2009**, *48*, 7514–7538.

(9) Popov, A. A. *J. Comput. Theor. Nanosci.* **2009**, *6*, 292–317.

(10) Zhang, J. F.; Fatouros, P. P.; Shu, C. Y.; Reid, J.; Owens, L. S.; Cai, T.; Gibson, H. W.; Long, G. L.; Corwin, F. D.; Chen, Z. J.; Dorn, H. C. *Bioconjugate Chem.* **2010**, *21*, 610–615.

(11) Fillmore, H. L.; Shultz, M. D.; Henderson, S.; Cooper, P.; Broaddus, W. C.; Chen, Z. J.; Chung-Ying, S.; Dorn, H. C.; Corwin, F.; Hirsch, J. I.; Wilson, J. D.; Panos, F. P. *Neuro-Oncol.* **2009**, *11*, 593–593.

(12) Ross, R. B.; Cardona, C. M.; Swain, F. B.; Guldi, D. M.; Sankaranarayanan, S. G.; Van Keuren, E.; Holloway, B. C.; Drees, M. *Adv. Funct. Mater.* **2009**, *19*, 2332–2337.

(13) Delgado, J. L.; Bouit, P. A.; Filippone, S.; Herranz, M. A.; Martin, N. *Chem. Commun.* **2010**, *46*, 4853–4865.

(14) Po, R.; Maggini, M.; Camaioni, N. *J. Phys. Chem.C* **2010**, *114*, 695–706.

(15) Ross, R. B.; Cardona, C. M.; Guldi, D. M.; Sankaranarayanan, S. G.; Reese, M. O.; Kopidakis, N.; Peet, J.; Walker, B.; Bazan, G. C.; Van Keuren, E.; Holloway, B. C.; Drees, M. *Nat. Mater.* **2009**, *8*, 208–212.

(16) Shustova, N. B.; Chen, Y. S.; Mackey, M. A.; Coumbe, C. E.; Phillips, J. P.; Stevenson, S.; Popov, A. A.; Boltalina, O. V.; Strauss, S. H. *J. Am. Chem. Soc.* **2009**, *131*, 17630–17637.

(17) Popov, A. A.; Shustova, N. B.; Svitova, A. L.; Mackey, M. A.; Coumbe, C. E.; Phillips, J. P.; Stevenson, S.; Strauss, S. H.; Boltalina, O. V.; Dunsch, L. *Chem. Eur. J.* **2010**, *16*, 4721–4724.
(18) Shustova, N. B.; Popov, A. A.; Mackey, M. A.; Coumbe, C. E.; Phillips, J. P.; Stevenson, S.; Strauss, S. H.; Boltalina, O. V. *J. Am. Chem. Soc.* **2007**, *129*, 11676–11677.
(19) Kareev, I. E.; Lebedkin, S. F.; Bubnov, V. P.; Yagubskii, E. B.; Ioffe, I. N.; Khavrel, P. A.; Kuvychko, I. V.; Strauss, S. H.; Boltalina, O. V. *Angew. Chem., Int. Ed.* **2005**, *44*, 1846–1849.
(20) Goryunkov, A. A.; Kuvychko, I. V.; Ioffe, I. N.; Dick, D. L.; Sidorov, L. N.; Strauss, S. H.; Boltalina, O. V. *J. Fluorine Chem.* **2003**, *124*, 61–64.
(21) Uzkikh, I. S.; Dorozhkin, E. I.; Boltalina, O. V.; Boltalin, A. I. *Dokl. Akad. Nauk* **2001**, *379*, 344–347.
(22) Shustova, N. B.; Kareev, I. E.; Kuvychko, I. V.; Whitaker, J. B.; Lebedkin, S. F.; Popov, A. A.; Chen, Y. S.; Seppelt, K.; H., S. S.; Boltalina, O. V. *J. Fluorine Chem.* **2010**, *131*, 1198–1212.
(23) Shu, C.; Cai, T.; Xu, L.; Zuo, T.; Reid, J.; Harich, K.; Dorn, H. C.; Gibson, H. W. *J. Am. Chem. Soc.* **2007**, *129*, 15710–15717.
(24) Kareev, I. E.; Popov, A. A.; Kuvychko, I. V.; Shustova, N. B.; Lebedkin, S. F.; Bubnov, V. P.; Anderson, O. P.; Seppelt, K.; Strauss, S. H.; Boltalina, O. V. *J. Am. Chem. Soc.* **2008**, *130*, 13471–13489.
(25) Popov, A. A.; Kareev, I. E.; Shustova, N. B.; Stukalin, E. B.; Lebedkin, S. F.; Seppelt, K.; Strauss, S. H.; Boltalina, O. V.; Dunsch, L. *J. Am. Chem. Soc.* **2007**, *129*, 11551–11568.
(26) Dorozhkin, E. I.; Ignat'eva, D. V.; Tamm, N. B.; Goryunkov, A. A.; Khavrel, P. A.; Ioffe, I. N.; Popov, A. A.; Kuvychko, I. V.; Streletskiy, A. V.; Markov, V. Y.; Spandl, J.; Strauss, S. H.; Boltalina, O. V. *Chem. Eur. J.* **2006**, *12*, 3876–3889.
(27) Darwish, A. D.; Abdul-Sada, A. K.; Avent, A. G.; Lyakhovetsky, V. I.; Shilova, E. A.; Taylor, R. *Org. Biomol. Chem.* **2003**, *1*, 3102–3110.
(28) Dorozhkin, E. I.; Goryunkov, A. A.; Ioffe, I. N.; Avdoshenko, S. M.; Markov, V. Y.; Tamm, N. B.; Ignat'eva, D. V.; Sidorov, L. N.; Troyanov, S. I. *Eur. J. Org. Chem.* **2007**, 5082–5094.
(29) Boltalina, O. V.; Galeva, N. A. *Russ. Chem. Rev.* **2000**, *69*, 609–621.
(30) Goryunkov, A. A.; Kareev, I. E.; Ioffe, I. N.; Popov, A. A.; Kuvychko, I. V.; Markov, V. Y.; Goldt, I. V.; Pimenova, A. S.; Serov, M. G.; Avdoshenko, S. M.; Khavrel, P. A.; Sidorov, L. N.; Lebedkin, S. F.; Mazej, Z.; Zemva, B.; Strauss, S. H.; Boltalina, O. V. *J. Fluorine Chem.* **2006**, *127*, 1423–1435.
(31) Campanera, J. M.; Heggie, M. I.; Taylor, R. *J. Phys. Chem. B* **2005**, *109*, 4024–4031.
(32) Boltalina, O. V.; Goryunkov, A. A.; Markov, V. Y.; Ioffe, I. N.; Sidorov, L. N. *Int. J. Mass Spectrom.* **2003**, *228*, 807–824.
(33) Troyanov, S. I.; Troshin, P. A.; Boltalina, O. V.; Ioffe, I. N.; Sidorov, L. N.; Kemnitz, E. *Angew. Chem., Int. Ed.* **2001**, *40*, 2285–2287.
(34) Neretin, I. S.; Lyssenko, K. A.; Antipin, M. Y.; Slovokhotov, Y. L.; Boltalina, O. V.; Troshin, P. A.; Lukonin, A. Y.; Sidorov, L. N.; Taylor, R. *Angew. Chem., Int. Ed.* **2000**, *39*, 3273–3276.
(35) Shustova, N. B.; Kuvychko, I. V.; Whitaker, J. B.; Larson, B. W.; Dunsch, L.; Chen, Y. S.; Seppelt, K.; Popov, A. A.; H., S. S.; Boltalina, O. V. *Chem. Commun.* **2010**, *47:3*, 875−877.
(36) Tagmatarchis, N.; Taninaka, A.; Shinohara, H. *Chem. Phys. Lett.* **2002**, *355*, 226–232.
(37) Shu, C.; Slebodnick, C.; Xu, L.; Champion, H.; Fuhrer, T.; Cai, T.; Reid, J. E.; Fu, W.; Harich, K.; Dorn, H. C.; Gibson, H. W. *J. Am. Chem. Soc.* **2008**, *130*, 17755–17760.
(38) Bingel, C. *Chem. Ber.* **1993**, *126*, 1957–1959.
(39) Hirsch, A.; Lamparth, I.; Karfunkel, H. R. *Angew. Chem., Int. Ed.* **1994**, *106*, 453–455.
(40) Hirsch, A.; Lamparth, I.; Groesser, T.; Karfunkel, H. R. *J. Am. Chem. Soc.* **1994**, *116*, 9385–9386.
(41) Cardona, C. M.; Kitaygorodskiy, A.; Echegoyen, L. *J. Am. Chem. Soc.* **2005**, *127*, 10448–10453.
(42) Kuvychko, I. V.; Whitaker, J. B.; Larson, B. W.; Shustova, N. B.; Raguindin, R. S.; Suhr, K. J.; Strauss, S. H.; Boltalina, O. V. *J. Phys. Chem. C* **2011** submitted.
(43) Popov, A. A.; Kareev, I. E.; Shustova, N. B.; Lebedkin, S. F.; Strauss, S. H.; Boltalina, O. V.; Dunsch, L. *Chem. Eur. J.* **2008**, *14*, 107–121.
(44) Shustova, N. B.; Popov, A. A.; Newell, B. S.; Miller, S. M.; Anderson, O. P.; Seppelt, K.; Bolskar, R. D.; Boltalina, O. V.; Strauss, S. H. *Angew. Chem., Int. Ed.* **2007**, *46*, 4111–4114.
(45) Kareev, I. E.; Shustova, N. B.; Kuvychko, I. V.; Lebedkin, S. F.; Miller, S. M.; Anderson, O. P.; Popov, A. A.; Strauss, S. H.; Boltalina, O. V. *J. Am. Chem. Soc.* **2006**, *128*, 12268–12280.
(46) Troyanov, S., I.; Goryunkov, A. A.; Dorozhkin, E. I.; Ignat'eva, D. V.; Tamm, N. B.; Avdoshenko, S. M.; Ioffe, I. N.; Markov, V. Y.; Sidorov, L. N.; Scheural, K.; Kemnitz, E. *J. Fluorine Chem.* **2007**, *128*, 545–551.
(47) Avdoshenko, S. M.; Goryunkov, A. A.; Ioffe, I. N.; Ignat'eva, D. V.; Sidorov, L. N.; Pattison, P.; Kemnitz, E.; Troyanov, S., I. *Chem. Commun.* **2006**, 2463–2465.
(48) Kareev, I. E.; Shustova, N. B.; Peryshkov, D. V.; Lebedkin, S. F.; Miller, S. M.; Anderson, O. P.; Popov, A. A.; Boltalina, O. V.; Strauss, S. H. *Chem. Commun.* **2007**, 1650–1652.
(49) Popov, A. A.; Dunsch, L. *J. Am. Chem. Soc.* **2007**, *129*, 11835–11849.
(50) Wakahara, T.; Iiduka, H.; Ikenaga, O.; Nakahodo, T.; Sakuraba, A.; Yoza, K.; Horn, E.; Mizorogi, N.; Nagase, S. *J. Am. Chem. Soc.* **2006**, *128*, 9919–9925.
(51) Porezag, D.; Frauenheim, T.; Kohler, T.; Seifert, G.; Kaschner, R. *Phys. Rev. B* **1995**, *51*, 12947–12957.
(52) Heine, T.; Vietze, K.; Siefert, G. *Magn. Reson. Chem.* **2004**, *42*, 199–201.
(53) Heine, T.; W., F. P.; Rogers, K. M.; Seifert, G. *J. Chem. Soc., Perkin Trans. 2* **1999**, 707–711.
(54) Cai, T.; Xu, L.; Gibson, H. W.; Dorn, H. C.; Chancellor, C. J.; Olmstead, M. M.; Balch, A. L. *J. Am. Chem. Soc.* **2007**, *129*, 10795–10800 and references therein.
(55) Cai, T.; Slebonick, C.; Xu, L.; Harich, K.; Glass, T. E.; Chancellor, C.; Fettinger, J. C.; Olmstead, M. M.; Balch, A. L.; Gibson, H. W.; Dorn, H. C. *J. Am. Chem. Soc.* **2006**, *128*, 6486–6492.
(56) Shustova, N. B.; Kuvychko, I. V.; Bolskar, R. D.; Seppelt, K.; Strauss, S. H.; Popov, A. A.; Boltalina, O. V. *J. Am. Chem. Soc.* **2006**, *128*, 15793–15798.
(57) Kareev, I. E.; Kuvychko, I. V.; Shustova, N. B.; Lebedkin, S. F.; Bubnov, V. P.; Anderson, O. P.; Popov, A. A.; Strauss, S. H.; Boltalina, O. V. *Angew. Chem., Int. Ed.* **2008**, *47*, 6204–6207.
(58) Stevenson, S.; Lee, H. M.; Olmstead, M. M.; Kozikowski, C.; Stevenson, P.; Balch, A. L. *Chem. Eur. J.* **2002**, *8*, 4528–4535.
(59) Shu, C.; Xu, W.; Slebodonick, C.; Champion, H.; Fu, W.; Reid, J. E.; Azurmendi, H.; Wang, C.; Harich, K.; Dorn, H. C.; Gibson, H. W. *Org. Lett.* **2009**, *11*, 1753–1756.
(60) Lee, H. M.; Olmstead, M. M.; Iezzi, E.; Duchamp, J. C.; Dorn, H. C.; Balch, A. L. *J. Am. Chem. Soc.* **2002**, *124*, 3494–3495.
(61) Olmstead, M. M.; Costa, D. A.; Maitra, K.; Noll, B. C.; Phillips, S. L.; Van Calcar, P. M.; Balch, A. L. *J. Am. Chem. Soc.* **1999**, *121*, 7090–7097.
(62) Alvarez, L.; Pichler, T.; Georgi, P.; Schwieger, T.; Peisert, H.; Dunsch, L.; Hu, Z.; Knupfer, M.; Fink, J.; Bressler, P.; Mast, M.; Golden, M. S. *Phys. Rev. B* **2002**, *66*, 035107/1–035107/7.
(63) Campanera, J. M.; Bo, C.; Olmstead, M. M.; Balch, A. L.; Poblet, J. M. *J. Phys. Chem. A* **2002**, *106*, 12356–12364.
(64) Valencia, R.; Rodriguez-Fortea, A.; Poblet, J. M. *J. Phys. Chem. A* **2008**, *112*, 4550–4555.
(65) Popov, A. A.; Dunsch, L. *Chem. Eur. J.* **2009**, *15*, 9707–9729.
(66) Popov, A. A.; Dunsch, L. *J. Am. Chem. Soc.* **2008**, *130*, 17726–17742.
(67) Checinska, L.; Troyanov, S. I.; Mebs, S.; Hubschle, C. B.; Luger, P. *Chem. Commun.* **2007**, 4003–4005.
(68) Bader, R. F. W. *Atoms in Molecules: A Quantum Theory*; Oxford University Press: Oxford, 1990.
(69) Bushmarinov, I. S.; Lyssenko, K. A.; Antipin, M. Y. *Russ. Chem. Rev.* **2009**, *78*, 283–302.

(70) Krause, M.; Dunsch, L. *ChemPhysChem* **2004**, *5*, 1445–1449.
(71) Elliott, B.; Yu, L.; Echegoyen, L. *J. Am. Chem. Soc.* **2005**, *127*, 10885–10888.
(72) Pinzon, J. R.; Plonska-Brzezinska, M. E.; Cardona, C. M.; Athans, A. J.; Gayathri, S. S.; Guldi, D. M.; Herranz, M. A.; Martin, N.; Torres, T.; Echegoyen, L. *Angew. Chem., Int. Ed.* **2008**, *47*, 4173–4176.
(73) Pinzon, J. R.; Gasca, D. C.; Sankaranarayanan, S. G.; Bottari, G.; Torres, T.; Guldi, D. M.; Echegoyen, L. *J. Am. Chem. Soc.* **2009**, *131*, 7727–7734.
(74) Pinzon, J. R.; Cardona, C. M.; Herranz, M. A.; Plonska-Brzezinska, M. E.; Palkar, A.; Athans, A. J.; Martin, N.; Rodriguez-Fortea, A.; Poblet, J. M.; Bottari, G.; Torres, T.; Gayathri, S. S.; Guldi, D. M.; Echegoyen, L. *Chem. Eur. J.* **2009**, *15*, 864–877.
(75) Jakes, P.; Dinse, K. P. *J. Am. Chem. Soc.* **2001**, *123*, 8854–8855.
(76) Rapta, P. A.; Popov, A. A.; Dunsch, L. *J. Phys. Chem. A* **2008**, *112*, 5858–5865.
(77) Neese, F. *Inorg. Chim. Acta* **2002**, *337*, 181–192.

NOTE ADDED IN PROOF

After this manuscript had been submitted, two X-ray structures of new $Sc_3N@C_{80}(CF_3)_{14}$ and $Sc_3N@C_{80}(CF_3)_{16}$ isomers with several CF_3-bearing THJs were reported (*Chem. Asian J.* **2011**, DOI: 10.1002/asia.201000661). In addition, the structure of dichlorophenyl derivative of $La@C_{3v}(7)$-C_{82} in which arene group is bonded to a THJ carbon atom was reported (*Angew. Chem. Int. Ed.* **2010**, *49*, 9715). These data show that in line with conclusions of this work, exohedral addition to THJ carbon atoms of endohedral metallofullerenes can be a common feature, in contrast to hollow higher empty fullerenes, in which such additions are "forbidden".